Exclusive electro-disintegration of tensor polarized deuterium

A Proposal to Jefferson Lab PAC 52

W. Boeglin[†]**, M. Sargsian**
Florida International University, FL

T. Horn, **C. Yero**[†]
The Catholic University of America, DC

E. Long[†], **S. N. Santiesteban**[†]
University of New Hampshire

I. P. Fernando[†]
University of Virginia, VA

M. Jones[†], **H. Szumila-Vance**[†]
Thomas Jefferson National Accelerator Facility, VA

April 29, 2024

[†]Spokesperson

Executive Summary

The most fundamental nuclear system is the deuteron, which has a wave function that is mostly dominated by the proton-neutron (pn) component. As such, it is a useful instrument for probing into different aspects of the pn strong interaction. The study of the pn system at short distances is one of these features, providing answers to basic questions in nuclear dynamics such as the relativistic description of nuclear structure, the dynamics of the repulsive core in nucleon-nucleon (NN) interactions, the importance of non-nucleonic degrees of freedom, and the transitions between hadrons and quarks at very short distances. Employing a tensor-polarized deuteron target in electro-production reactions opens up new avenues for investigating various phenomena in short-range hadronic and nuclear physics.

In addition, pn potentials, such as AV18 and CD-Bonn exhibit notable disparities in their projections at high momentum, which corresponds to small inter-nucleon distances. Theoretical studies suggest that these differences could be identified and measured using specialized electro-disintegration experiments that utilize a tensor target.

We propose to measure the exclusive tensor-polarized electro-disintegration of the deuteron in Hall C. An 11-GeV electron beam will be incident on a solid 3-cm long tensor-polarized ammonia (ND_3) target. The scattered electrons will be detected by the Super High Momentum Spectrometer (SHMS) in coincidence with the knocked-out protons detected by the High Momentum Spectrometer (HMS), and the recoil ("missing") neutrons will be reconstructed from momentum conservation. We will focus in the kinematic region that covers $1.5 < Q^2 < 2.5$ GeV^2, missing momentum $0.1 < P_m < 0.5$ GeV, and recoil angle $0 < \theta_{nq} < 90°$.

We will measure the tensor asymmetry A_{zz} and we will extract $A_{node} = 1 + \frac{2A_{zz}}{(3\cos^2\theta_N - 1)}$. The tensor asymmetry A_{zz} and A_{node} will allow us to distinguish between the AV18 and CD-Bonn NN potentials. Additionally, $A_{node} \sim U(P_m)^2 + 2\sqrt{2}U(P_m)W(P_m)$ will allow us to access two nodes: i) $U = -2\sqrt{2}W$ and ii) $U = 0$. This measurement will provide a novel test of our understanding of the S- and D-waves, and will help us to evaluate the NN potentials in a region of significant disagreement.

Although the differences between the two NN potentials might seem small, both parameterizations predict significantly different strengths for high momenta above 400 MeV, especially for the D component. The strong predominance of np short-range correlations (SRCs), which are associated with the tensor component of NN interaction inside SRCs, has increased the motivation to understand the momentum distribution of the D-wave. The high-momentum part of the nuclear wave function where the tensor interaction predominates could have a substantial impact on the dynamics of asymmetric nuclei and have important consequences for superdense nuclear matter and neutron stars.

We request a total of 82 PAC days with 11 GeV beam energy, which consists of 56 PAC days of physics production and 26 PAC days of overhead. This work will complement and contribute to Jefferson Lab's larger tensor effort, which continues to draw interest from the theoretical spin, polarized target, and experimental spin groups.

Contents

1 Motivation

The deuteron is the simplest composite nucleus consisting of one proton (p) and one neutron (n). Despite its apparent simplicity, it represents a unique "laboratory" for exploration of the structure of strong interaction at different distance scales with the possibility of probing limits of nucleonic degrees of freedom. The importance of understanding of the deuteron structure at large internal momenta has increased with the observation of the strong pn dominance of two-nucleon short range correlations (SRC) in medium and heavy nuclei [1,2]. The pn dominance in 2N SRCs led to the prediction of the momentum sharing effect [3] according to which the minority component in asymmetric nuclei have larger share of high momentum component of nuclear wave function. The later was confirmed experimentally in $(e, e'p)$ experiments at Jefferson Lab [4,5]. As such, the mentioned nuclear effects relate the understanding of the dynamics of the high momentum component of the deuteron wave function to the dynamics of high density asymmetric nuclear matter, making the scope of the problems that deuteron studies can address very broad.

Contemporary studies of the deuteron address the following *outstanding* issues using the advanced high energy capabilities of Jefferson Lab:

- Even though the partial waves in the deuteron are not directly observable [6,7], they define the high momentum structure of the wave function and the relative strength of the S- and D-waves in the deuteron predicted within different realistic NN potentials [8–11] significantly differ at internal momenta above ~ 400 MeV/c.

- The role of relativistic effects is expected to become important at internal momenta comparable to the nucleon rest mass. However, despite many decades of theoretical studies [12–15], no definitive results is achieved in understanding the role of the relativity in the dynamics of the deuteron.

- Dynamics of the nuclear repulsive core; It is understood that stability of atomic nuclei and emergence of saturation density in the nuclear matter is predominantly related to the S-channel repulsion in the NN system. However due to lack of systematic data in high energy NN scattering the dynamical origin of nuclear repulsion is practically unknown. QCD allows an existence of very rich dynamics generating a nuclear repulsion [16–19] that includes emergence of non-nucleonic states including hidden color component in the deuteron. In this respect while the D-wave in the deuteron is sensitive to the strength of the tensor interaction in the pn channel, the S-state at large momenta is predominately due to the nuclear core.

- Limits of nucleonic degrees of freedom; existence of rich baryonic spectrum is expected to provide an emergence of non-nucleonic components in the bound pn system with an increase of the internal momentum in the deuteron. In fact within the framework of the six-quark model one expects $\Delta\Delta$ and hidden color components to dominate significantly the pn component (see e.g. [17]). Discovering the limits of pn component in the deuteron and dynamics of its transition to non-nucleonic components will provide an important knowledge in understanding the similar phenomena in high density cold nuclear matter relevant for example to the dynamics of the cores in neutron stars.

1.1 High Energy Experiments Involving Deuteron

1.1.1 Elastic and Inclusive Processes

There were significant efforts in investigation of the structure of the deuteron at high energy and momentum transfer electronuclear processes started at SLAC and continued in Jefferson Lab. The first experiments at SLAC measured deuteron form-factors at large Q^2 as well as its structure functions in inclusive $d(e,e')X$ reactions at smaller values of transferred energy which were most sensitive to the high momentum component of deuteron wave function. The similar strategy was pursued also in Jefferson Lab experiments with significant amount of high quality data being accumulated in the process.

The details of elastic scattering experiments are discussed in Ref. [20] while inclusive processes reviewed in Ref. [21]. Theoretical analysis of the elastic scattering data demonstrated that the detection of the scattered deuteron corresponds to the integration of the final state deuteron wave function over the internal momentum range. As a result, elastic scattering is a very indirect method to probe the initial deuteron state at large internal momenta. Also the strong dominance of the deuteron at small internal momenta allowed in principle a sizable contribution from long range hadronic exchange currents.

Inclusive processes at $x_{Bj} > 1$ provided the best access to the large momentum component in the deuteron however the measured cross section was related to the high momentum distribution in the deuteron integrated over the transverse momentum of bound nucleon. These experiments however revealed sizable high momentum component in the deuteron.

1.1.2 Exclusive Electro-Disintegration Processes

A new age of exploration of the deuteron started with completion of first high Q^2 exclusive experiments in which high missing momenta were measured in $d(e,e'p)n$ reactions in which proton was clearly identified as a struck nucleon that carries almost all transferred to the deuteron momentum [22, 23].

The advantage of these reactions in high Q^2 is that the long range processes such as meson-exchange current (MEC) and isobar contributions (IC) are suppressed due to large Q^2 and choosing the kinematic in which $x_{Bj} > 1$ moving away from the threshold of Δ-isobar production [24].

Remaining effects that impede the direct probe of high momentum component of the deuteron is final state interaction of struck and recoil nucleons both in the direct and charge-interchange channels. However the advantage of high energy processes in this case is that one can apply eikonal approximation in evaluation of final state interaction (FSI) effects. There have been significant theoretical efforts in calculation of FSI effects in deuteron electrodisitengration processes by several groups [25–32]. One of the important results of these studies was that due to eikonal regime of the rescatterings FSI was localized in transverse direction of the production of recoil nucleon (Fig. 1). As Fig. 1 demonstrates, there is a prediction of a kinematic window of the recoil nucleon angle relative to the momentum transfer q, θ_{nq}, in which FSI is a small contribution, which allows its use in probing the high momentum part of the deuteron momentum distribution.

This expectation was confirmed in the high precision experiment of Hall A, which allowed a direct measurement of the deuteron momentum distribution up to 550 MeV/c at $Q^2 =$

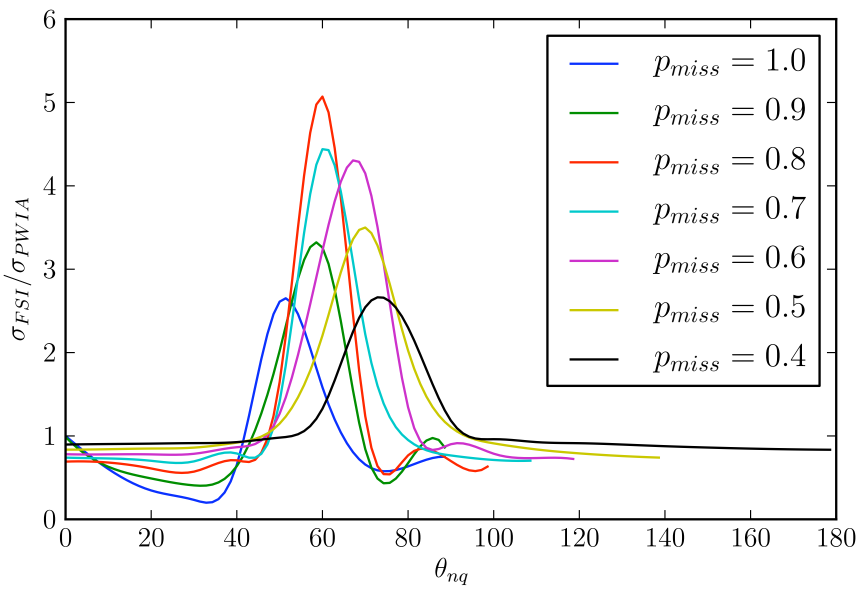

Figure 1: Ratios of the calculated cross sections including FSI effects to the cross sections calculated within PWIA at different values of missing momenta as a function of the neutron recoil angle.

3.5 (GeV/c)^2. As Fig. 2 shows for recoil angles of $\theta_{nq} = 35°$ and $45°$, the effects from FSI are a small contribution that allows a discrimination between two (Paris and CD-Bonn) different models of deuteron wave function.

A similar approach was used in the recent Hall C experiment [33] to extend the probe of the deuteron internal momentum above 550 MeV/c. The results were rather unexpected. As Fig. 3 shows, while reproducing the result of Hall C experiment for $p_m \leq 550$ MeV/c, the measured reduced distribution qualitatively disagrees with any known model of the deuteron wave function for $p_m \geq 750$ MeV/c.

Such a disagreement can be attributed to an enhanced role of the relativistic effects as well as a possible indication of the onset of non-nucleonic degrees of freedom since $p_m \approx$ 750 MeV/c corresponds to the inelastic threshold in the pn channel [34].

In any case, the discussed data demonstrate the advantage of using high Q^2 exclusive disintegration of the deuteron in probing the high momentum component of the deuteron momentum distribution at unprecedentedly large internal momenta.

1.2 Exclusive Electro-Disintegration Processes of Tensor-Polarized Deuterons

While exclusive electrodisintegration of the deuteron allows access to unprecedentedly large internal momenta in the deuteron, it does not allow investigation into the relative role of the partial waves in the deuteron.

The existence of S- and D- partial waves in the deuteron originates from the non-relativistic description of the deuteron. The deuteron has a total spin of $J = 1$ with positive parity, P. In the non-relativistic framework, due to the relation of $P = (-1)^l$, one identifies only

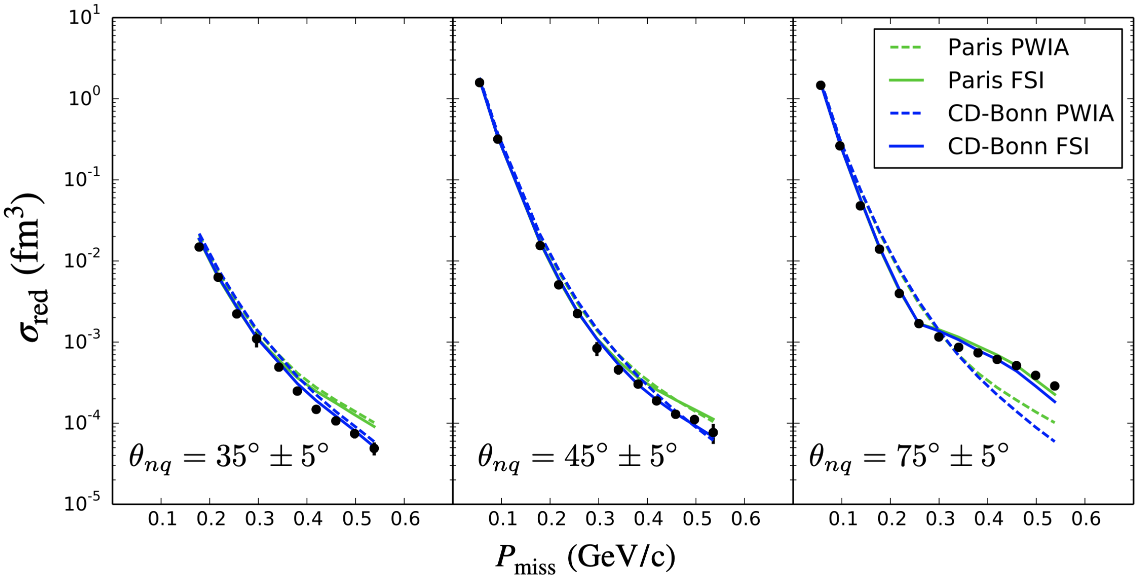

Figure 2: The experimental reduced cross sections (momentum distributions) [23] for three values of the recoil angle θ_{nq}. The solid lines are calculations [31] including FSI and the dashed lines correspond to PWIA calculations.

two partial, S- and D-, wave components, in the deuteron wave function. The latter being responsible for the quadruple momentum of the deuteron.

In the relativistic case, more structures are allowed in the deuteron and some of them are associated with non-nucleonic degrees of freedom. The current qualitative "map" of the understanding the deuteron can be presented similar to Fig. 4. Within a non-relativistic description, the momentum distribution is the sum of the partial S- and D- wave distributions in which D- wave defines the high momentum component of the deuteron for up to $\sim$ 700 MeV/c and apparently with the emergence of the repulsive core effect (since repulsion is in the S-channel) the S-wave should dominate for internal momenta above 700 MeV/c. However the latter statement is rather qualitative since in this region one expects significant relativistic as well as possible non-nucleonic component effects.

It is worth to emphasize that previous experiments established two important facts about the structure of the deuteron: first, for up to 650 MeV/c deuteron consists of proton and neutron only [23, 33] and, secondly, the D-wave dominates the high momentum distribution in the region of $300-600$ MeV/c. It is interesting that the latter observation comes from the observation of the strong pn-dominance in 2N SRCs since tensor forces do not result in pp and nn short range correlations. Even though this dominance is experimentally established, the strength of the D-wave is not well known for the considered range of momenta. The deuteron electrodisintegration processes [23, 33] support deuteron wave function calculated by CD-Bonn potential while 2N SRC studies within generalized contact formalism [35–37] support the pn- SRCs with AV18 potential. As it follows from Fig. 4, the V18 and CD-Bonn [10] potentials predict substantially different strength of D-wave in the $300-600$ MeV/c internal momentum region.

The way to isolate the D- wave contribution is to consider the scattering from tensor

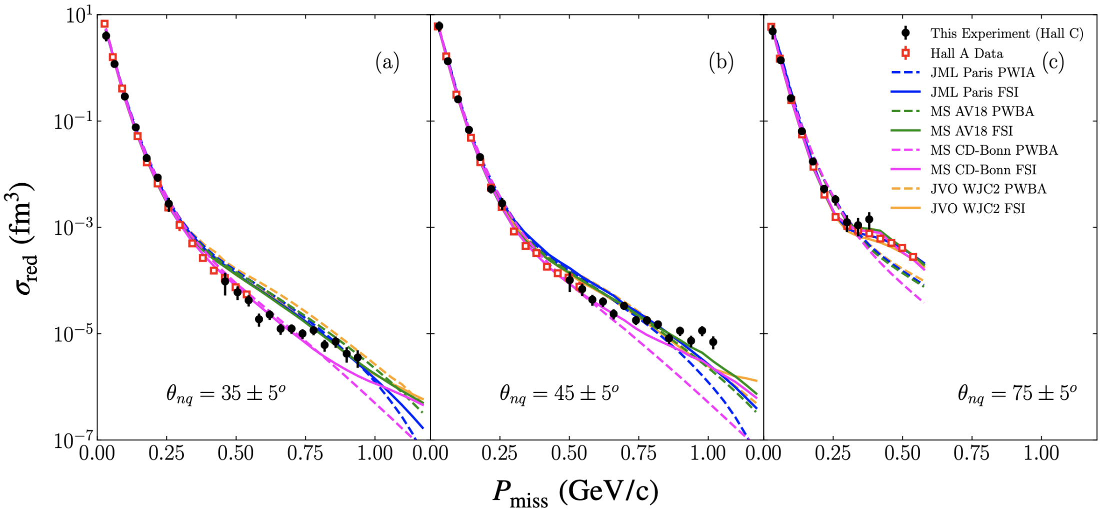

Figure 3: The experimental reduced cross sections (momentum distributions) for three values of the recoil angle θ_{nq} [33]. The solid lines are calculations including FSI and the dashed lines correspond to PWIA calculations [31].

polarized target. In this case, within plane wave impulse approximation, one measures the the quantity:

$$+\rho_{20}(p,\theta_p) \equiv \frac{|\psi_d^1|^2 + |\psi_d^{-1}|^2 - 2|\psi_d^0|^2}{3} = \frac{3\cos^2(\theta_p) - 1}{2}\left[2\sqrt{2}u(p)w(p) - w^2(p)\right], \quad (1)$$

where ψ_d^m- represents a deuteron wave function with polarization $m = -1, 0, 1$ and θ_p is the direction of internal momenta with respect to the polarization axis of the deuteron. As above equation shows, the $u(p)^2$ contribution to ρ_{20} drops out resulting in a sensitivity to the D- wave distribution $w(p)$. For practical consideration it is convenient to discuss the asymmetry defined as:

$$A_{20}(p,\theta_p) = \frac{\rho_{20}(p,\theta_p)}{\rho_{unp}(p)} \quad (2)$$

where

$$\rho_{unp}(p) = u(p)^2 + w(p)^2. \quad (3)$$

In Fig. 5 predictions for $A_{20}(p, \theta_p = 0)$ are presented for deuteron wave function calculated using Paris [9], V18 [8] and CD-Bonn [10] potentials.

Uniqueness of tensor polarized deuteron is that while the momentum distribution of the unpolarized deuteron is primarily dominated by the $u(p)$ contribution at low relative momentum, as illustrated in Fig. 4, the strength of tensor polarization diminishes at small momenta since $w(p = 0) = 0$ (see Eq. 1). As a result asymmetry A_{20} is sensitive to the higher internal momentum of the deuteron and the dynamics of poorly known D- partial wave. Fig. 5 shows that the predictions diverge starting $p \geq 300$ MeV/c that allows to identify the valid potential of NN interaction without large contribution from relativistic effects. As such it is a potential tool to verify the validity of pn interaction model at short distances [38].

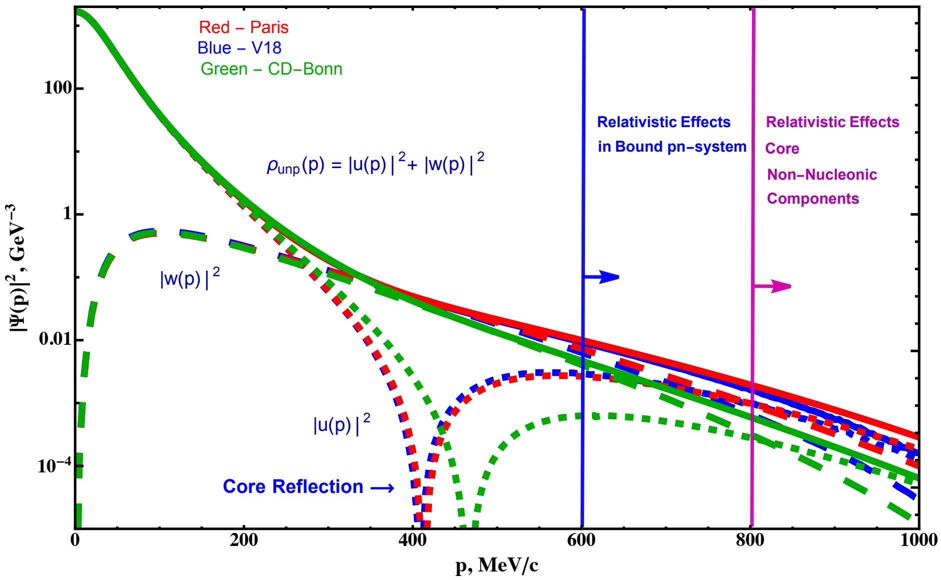

Figure 4: Momentum distributions for S (dotted) and D (dashed) partial waves as well as their total contribution to unpolarized deuteron momentum distribution (solid). Distributions are for deuteron wave function calculated with Paris, CD-Bonn and V18 potentials.

1.2.1 Probing NN Core in the Deuteron

One of the implications of the existence of short range repulsion in the S- channel is the appearance of the node in the momentum space distribution of the radial wave function. This is seen for the S-partial wave of the deuteron in Fig.4 at $p \sim 400$ MeV/c. However as figure shows the node is masked by the strong dominance of the D-wave at the same momentum region.

Availability of polarized target gives a unique opportunity to isolate to isolate the S-state by combining unpolarized and tensor polarized measurements in such a form that results in:

$$\rho_{node}(p) = \rho_{unp}(p) + \frac{2\rho_{20}}{3\cos^2(\theta_p) - 1} = u^2(p) + 2\sqrt{2}u(p)w(p) \tag{4}$$

For practical purposes it is convenient to consider the new asymmetry defined as:

$$A_{node}(p) \equiv \frac{\rho_{node}(p)}{\rho_{unp}} = 1 + \frac{2A_{20}(p,\theta_p)}{3\cos^2(\theta_p) - 1} = \frac{u^2(p) + 2\sqrt{2}u(p)w(p)}{u(p)^2 + w(p)^2}. \tag{5}$$

As it follows from Eqs.(4) and (5) the asymmetry $A_{node}(p)$ will become zero once the node of the S-wave is probed. Fig. 5 shows large sensitivity to the position of these node to the choice of the potential on calculation of the deuteron wave function at $p \geq 400$ MeV/c. Note that A_{node} has another zero at $p \approx 180$ MeV/c which corresponds to the condition of

$$u(p) = -2\sqrt{2}w(p). \tag{6}$$

Since internal momentum for the above relation is not large the observation of this node will help in the calibration of the measurement.

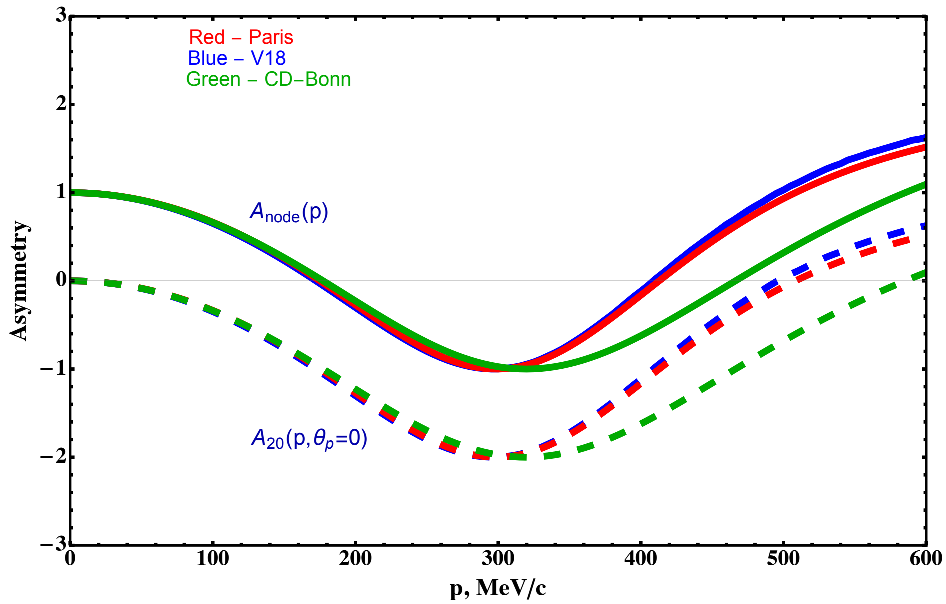

Figure 5: Momentum distributions for S (dotted) and D (dashed) partial waves as well as their total contribution to unpolarized deuteron momentum distribution (solid). Distributions are for deuteron wave function calculated with Paris, CD-Bonn and V18 potentials.

1.2.2 Final State Interaction and Relativistic Effects

The above discussed approach of probing the D-partial wave and the node of the S- wave distributions assumes no final state interaction present in the exclusive electrodisintegration process. Thus to accomplish such a program one needs to identify a kinematics in which FSI is not large and preserves the features of asymmetries discussed in the previous sub-sections.

In this case the great advantage is the high energy kinematics of the reaction in which case eikonal regime is established for FSI. As it was discussed in Sec. 1.1.2 due to strong angular anisotropy of FSI one can choose specific kinematics to suppress FSI (see Fig. 1.) To evaluate the FSI effects one used the calculation based on virtual nucleon approximation [31] which previously described data of high Q^2 electrodisintegration process for unpolarized deuteron target [22, 23, 33] for up to 600 MeV/c of missing momenta.

In Figure 6 the calculation of angular distribution of tensor asymmetry A_{zz} is presented (note that in PWIA A_{zz} coincides with A_{20} discussed in the previous sections. In general A_{zz} contains contributions from electron-bound nucleon interaction which does not cancel when FSI are present.). The figure shows the tensor asymmetry with respect to the neutron recoil angle θ_{nq} for a 0.4 GeV missing momenta and $Q^2 = 3.5$ GeV^2/c^2. It can be seen that at low angles (parallel kinematics) the FSI are minimal, and the theory predicts a distinct differentiation between the AV18 and CD-Bonn potentials. Experimental data to probe such predictions does not exist, and there is only one inclusive experiment approved in Jefferson Lab to probe the tensor asymmetry. Although the inclusive data will be extremely valuable to constrain the theory, it does not have the sensitivity to the np pair initial configuration, and therefore, a clean isolation to kinematic regions where FSI are minimal is not possible.

What concerns to the relativistic effects, the current proposal confines its measurement to

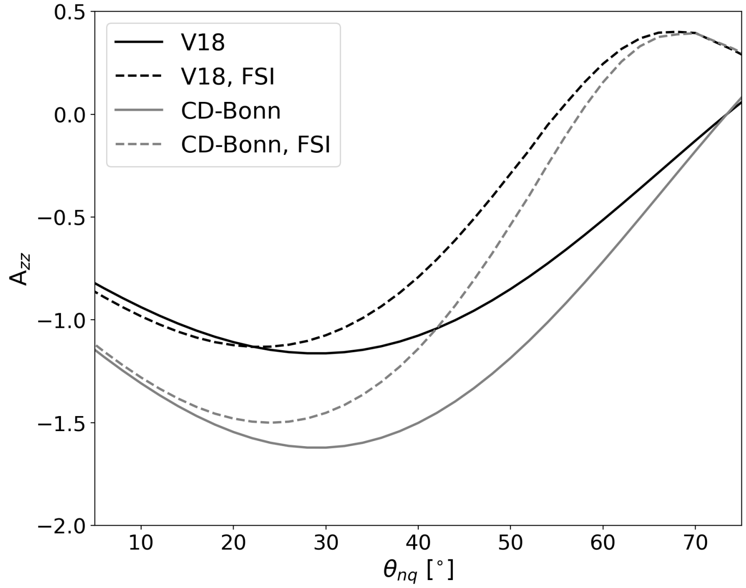

Figure 6: Tensor asymmetry (A_{zz}) with respect to the neutron recoil angle θ_{nq} for a 0.4 GeV missing momenta and $Q^2 = 3.5$ GeV^2/c^2. Figure from [39] shows that a θ_{nq} the FSI effects are smaller and the V18 and CD-Bonn differences can be distinguished.

up to 500 MeV/c for which the recent studies of electrodisintegration processes as well as 2N SRCs in nuclei demonstrated that the pn component is the only component in the deuteron with negligible possible contribution for non-nucleonic degrees of freedom. Based on the analysis of the recent electrodisintegration data they are expected to be moderate contributing mainly to the extreme co-linear kinematics [38] in which recoil nucleon produced in 180^0 with respect to the momentum transfer. Such relativistic effects can be accounted within light-front (LF) approach for which is currently being developed for electrodisintegration reactions [34, 40].

It is worth mentioning that tensor polarized target at extremely large missing momenta ($>$ 800 MeV/c) provides a very sensitive probe to the existence of non-nucleonic components in the deuteron [34] which represents an important extension to the current proposal.

Finally it is worth emphasizing that asymmetry measurements are an advantage with respect to the cross section measurement in relation to possible modification of the bound nucleon structure since in this case elementary eN cross section largely cancels out. This is especially the case for the proposed range of internal momenta for which no significant contribution from non-nucleonic components in the deuteron is expected.

1.2.3 Previous Measurements

Because of the difficulties involved in constructing and operating a polarized deuterium target within an electron beam, there have been only a limited number of electro-disintegration experiments conducted to date. An experiment conducted at NIKHEF [41] observed the vector analyzing power A^V for missing momenta up to approximately 350 MeV/c at $Q^2 \geq 0.21$ GeV^2/c^2 for quasielastic scattering of polarized electrons from vector-polarized deuterium.

This experiment demonstrated the influence of the D-state in the deuteron wave function on the missing momentum. Particularly, for missing momentum larger than 200 MeV/c, the D-state was found to be predominant. It also showed increasing sensitivity to isobar configurations and FSI with increasing missing momentum.

The first measurement of the tensor asymmetry in electro-disintegration at NIKHEF used a polarized gas target and measured missing momentum up to 150 MeV/c [41]. The data seem to be described by a calculation that includes the effects of final-state interaction, meson-exchange and isobar currents, and leading-order relativistic contributions. Even for this small Q^2 value, the PWIA description by Sargsian [39], given by Glauber approximation and eikonal treatment for FSI, is the same order of magnitude as the data and describes the missing momentum behaviour.

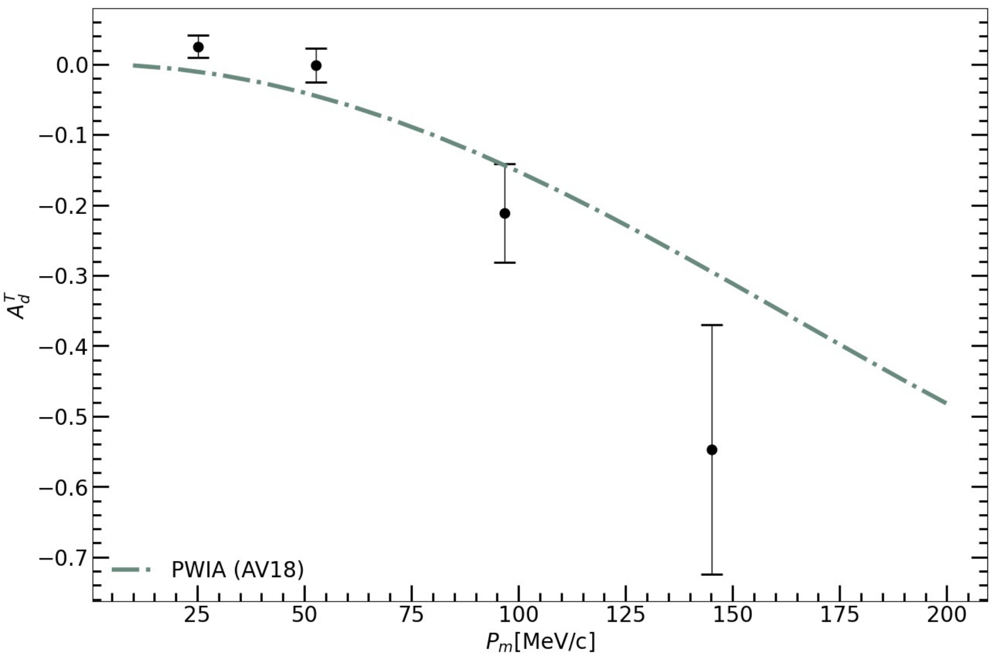

Figure 7: Sargsian [39] description of the NIKHEF data [41] with the PWIA approximation.

The second and latest measurement of the tensor asymmetry was done by the Bates collaboration [42, 43] up to missing momentum of 500 MeV/c. Data were collected simultaneously over a momentum transfer range of $0.1 < Q^2 < 0.5$ GeV$^2/c^2$. Our proposed measurement will access higher missing momenta and provide strong constraints on theoretical models.

2 Experimental Concept

We will focus the spectrometers in the $1.4 < Q^2 < 2$ GeV^2 region, which will enable a more accurate description from the eikonal approximation, and we will probe nucleons with momentum up to 500 MeV/c [44, 45]. We will reduce FSI contributions by a choice of parallel kinematics (relative the $q-$vector). Under these conditions, we will be significantly more sensitive to the choice of the NN potential than in the unpolarized experiments.

This experiment is planned to take place in Hall C, utilizing the High Momentum Spectrometer (HMS) and the Super High Momentum Spectrometer (SHMS). We will need an ND_3 polarized target with tensor enhancement, with the magnetic field oriented at an angle $\theta_B = 20°$ from the z-axis toward the HMS, as illustrated in Fig. 8. We will also use the Hall C Moller Polarimeter to measure the polarization of the electrons, a chicane magnet at the entrance of the scattering chamber to steer the electrons [46, 47]. Additionally, we will require the slow raster and to operate with currents from 50-100 nA.

2.1 Overview

The One-Photon Exchange approximation (OPE) describes deuteron electro-disintegration as the process where an electron interacts with the deuteron through the exchange of a virtual photon, resulting in the deuteron breaking up into a proton and a neutron, as illustrated in Fig. 8. The scattered electron (k_f,θ_e) will be detected by SHMS in coincidence with the knocked-out proton (p_f,θ_p) in the HMS. The recoil ("missing") neutron (P_miss, θ_{nq}) is reconstructed from momentum conservation.

The particular kinematic requirements for this proposal requires a proton detection angle of $> 35°$, which exceeds the target magnet minimum opening angle of ± 35 degrees in the longitudinal (+z) direction. This restriction imposes an upper limit on both spectrometers' central detection angles. Therefore, it is necessary to rotate the target magnetic field orientation to $\theta_B = 20°$ to accommodate a maximum spectrometer angle of $\theta_{\mathrm{HMS,max}} = 55°$ and $\theta_{\mathrm{SHMS,max}} = 15°$ as specified in Fig. 8. The central spectrometer kinematics are summarized in Table 1. However, due to a finite spectrometer acceptance, the central kinematics may not reflect the actual kinematics distributions. For a full description of the proposed kinematics, see section 3.3.1.

	k_f (GeV/c)	θ_e (deg)	p_f (GeV/c)	θ_p (deg)	P_miss (MeV/c)	Q^2 (GeV/c)^2
central setting	9.0	7.61	1.520	52.34	–	–
kinematic coverage	9.9–10.3	6–9	1.35–1.7	50–55	10-500	1.5–2.5

Table 1: Central and full spectrometer kinematics coverage for an incident electron beam energy of $E_b = 11$ GeV.

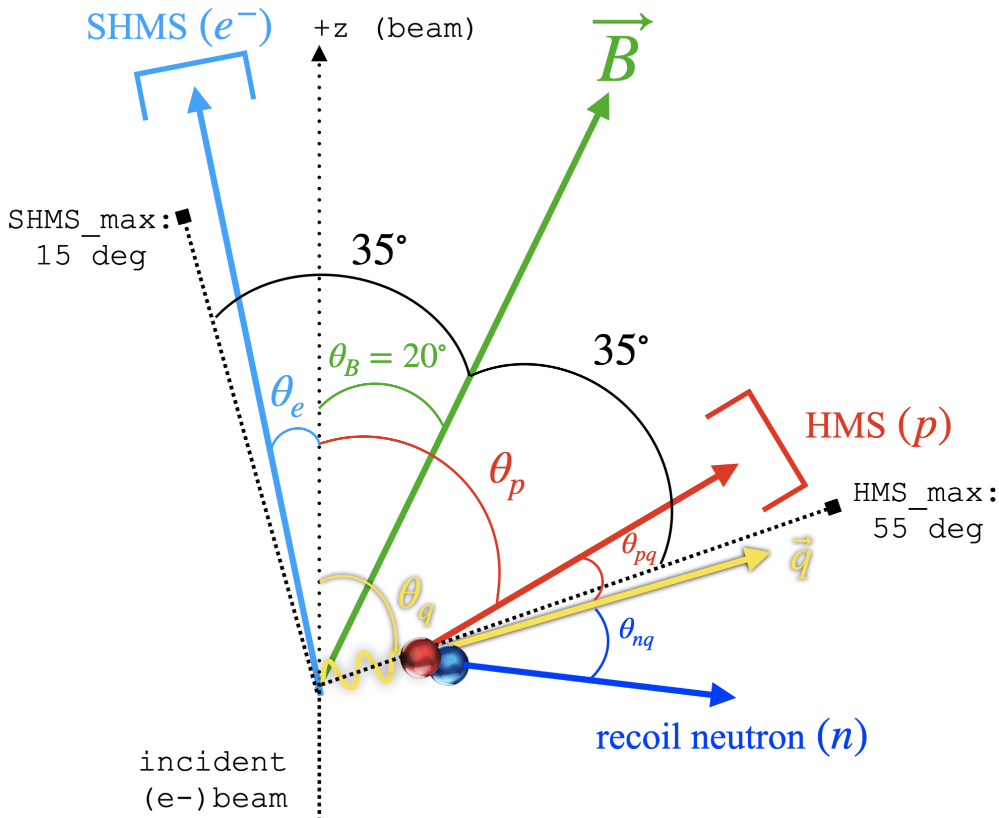

Figure 8: Schematic diagram of spectrometer kinematics setup

2.2 Polarized Target

The target utilized for this experiment will be the same target as for the upcoming inclusive tensor measurements of b_1 and A_{zz} [48,49], although it will be oriented at 20° with respect to the beam line rather than longitudinal to it. The target will be operated with a slow raster and beamline instrumentation capable of characterizing a low current (50-100 nA) beam. The target material will be deuterated ammonia (ND_3), which will be held at a temperature of 1 K with a liquid helium evaporation refrigerator and at a magnetic field of 5 T utilizing the new Hall C target magnet, which is shown in Fig. 9. This magnet has a ±35° opening in the longitudinal direction and a ±25° opening in the transverse direction, and for this experiment will operate with the ±35° longitudinal opening. The target material will be beads of frozen ND_3 with a packing fraction of approximately 65% that are held in 3 cm long, 1.5 cm radius target cups.

The vector (P) and tensor (Q) polarizations can be described by the populations (ρ) of the $m_s = 0, \pm 1$ spin states with a quantization axis along the magnetic holding field such that

$$\begin{aligned} P &= \rho_+ - \rho_-, \\ Q &= (\rho_+ + \rho_-) - 2\rho_0 = 1 - 3\rho_0. \end{aligned} \tag{7}$$

The target vector polarization is enhanced via Dynamic Nuclear Polarization (DNP), where microwaves will be used to drive the hyperfine transitions to align the nuclear spins into the

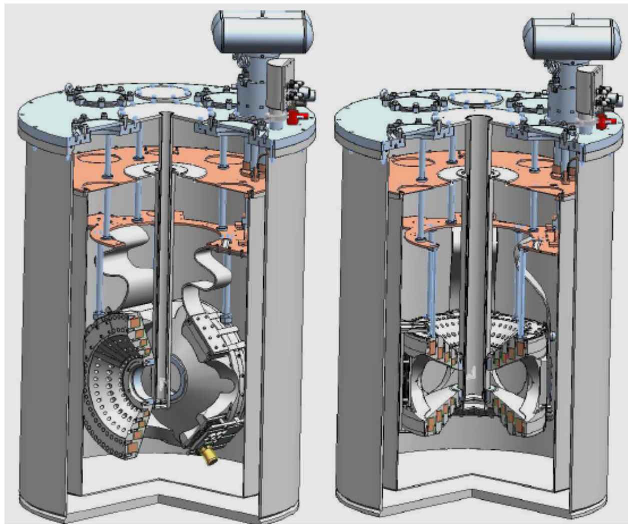

Figure 9: Cut-away images of the new Hall C target magnet, which shows the cutaway for both the longitudinal (left) and transverse (right) orientations. Figure courtesy of C. Keith.

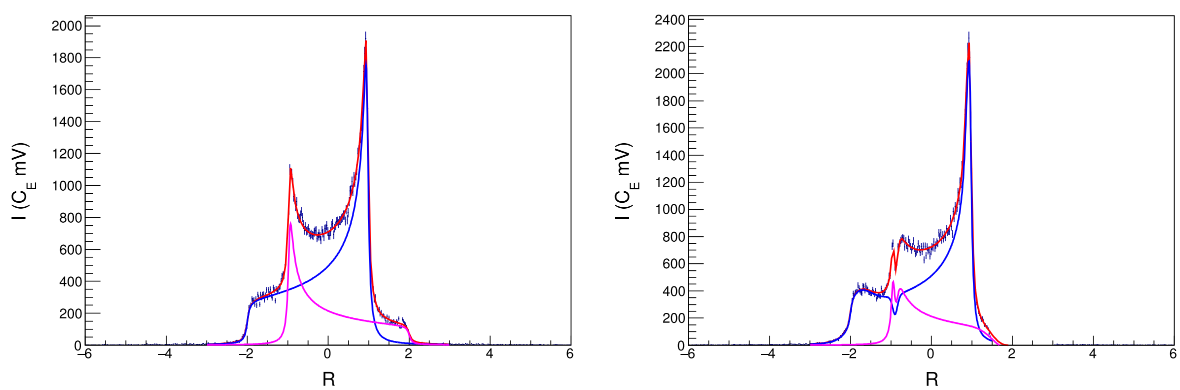

Figure 10: Left shows a DNP-enhanced deuteron NMR signal with vector polarization of $P =$ 49.8%. Right shows a deuteron NMR signal where tensor polarization has been enhanced to $Q = 28.8\%$ by utilizing ssRF on the DNP-enhanced signal. Suppression of tensor polarization to $Q \approx 0$ can also be achieved by applying ssRF on the opposite peak and shoulder. Figures are from [50].

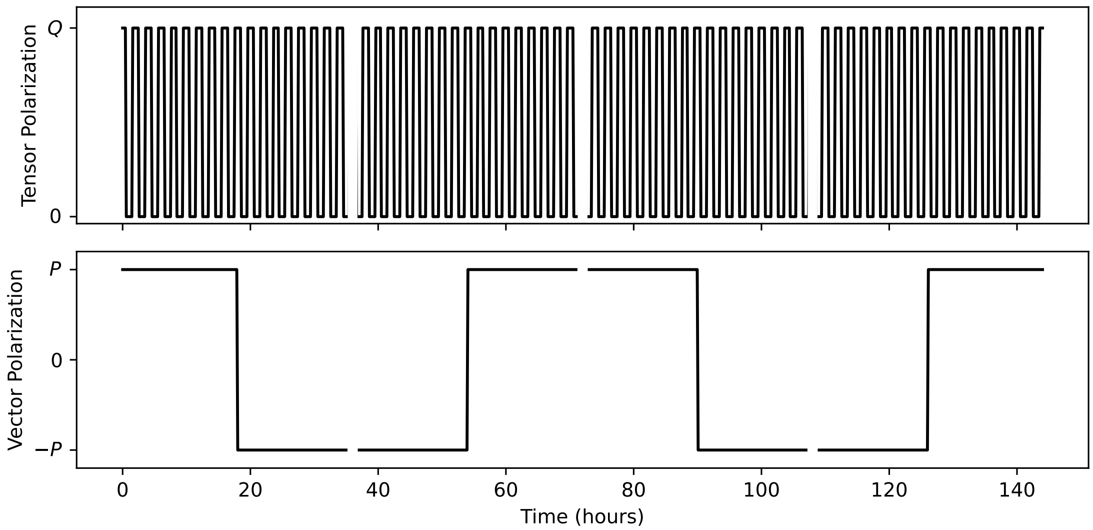

Figure 11: A visualization of the 72-hour polarization cycle that will be used to reduce time-dependent systematic effects. Here the tensor polarization flip is shown every 2 hours to make it visible, though in the experiment it will be flipped each hour.

$m = \pm 1$ states. This will inherently cause an increase of tensor polarization by filling the $\rho_\pm$ populations, which creates an equilibrium tensor polarization of

$$Q_{eq} = 2 - \sqrt{4 - 3P^2}. \tag{8}$$

From this, the tensor polarization can be either further enhanced or suppressed utilizing semi-selective RF saturation [50, 51], where an additional RF manipulation is performed on sections of the deuteron's NMR line, as shown in Fig. 10. This technique will allow cycles of tensor polarization between $Q_{eq} = 0\%$ to $+27\%$ that can be cycled each hour while maintaining high vector polarizations of $P = \pm 50\%$ for multiple days. The more rapid cycling of tensor polarization can be utilized to mitigate effects from detector and beamline drifts by combining the tensor enhanced states over both $\pm P$ vector polarization states, and similarly for the tensor suppressed states. Both vector and tensor polarizations will be measured by fitting the deuteron lineshape as described in [50, 52], which will have an expected relative uncertainty of $\pm 7\%$.

The heating of the target material by the beam will cause a drop of a few percent in the polarization, and the polarization will slowly decrease with time due to radiation damage. Most of this radiation damage can be repaired by periodically annealing the target until the total dose on the material is greater than approximately 5×10^{15} e/cm^2, at which time the material will be replaced. Dedicated runs for measuring the thermal equilibrium (TE) polarization without DNP will be taken to ensure accuracy of the polarization extraction from lineshape fitting. Similarly, dedicated runs will be taken to measure the target packing fraction and dilution factor, as well as runs with an empty target cup to remove background scattering.

2.3 Chicane

The polarization direction will be oriented 20°to the beam axis throughout the experiment. This setup will cause a deflection of the electrons, necessitating the use of a chicane to maintain proper beam transport. Jay Benesch has developed a new chicane that is expected to meet the requirements for compensating the bending caused by the target field. According to a previous technical note and supplement [46, 47]., it is probable that the current 2 cm vertical chicane in Hall C will be adequate for the necessary bending in this experiment.

3 Proposed measurement

In the following section we describe the observable, the expected kinematic coverage from simulations and the expected results. It's essential to clarify that in this context, A_{zz} refers to the asymmetry A_{20} to maintain consistency with the approved inclusive proposals [48,49].

3.1 A_{zz} experimental method

The measured double differential cross section for electron scattering from a spin-1 target is characterized by a vector polarization P and tensor polarization Q. After integrating over the beam polarization, the cross section can expressed as [53]

$$\frac{d^6\sigma_p}{dE_{e'}d\Omega_{e'}dE_p d\Omega_p} = \sigma_u \left[1 + PA_d^V + \frac{1}{2}QA_{zz}\right], \tag{9}$$

where σ_u is the unpolarized cross section. A_d^V is the vector asymmetry and A_{zz} is the tensor asymmetry.

This experiment aims to probe the tensor asymmetry by using four polarization states:

$$A_{zz} = \frac{2}{P_{zz}}\left(\frac{\sigma(P,Q) + \sigma(-P,Q)}{\sigma(P,0) + \sigma(-P,0)} - 1\right), \tag{10}$$

where $\sigma(P,Q)$ and $\sigma(-P,Q)$ require tensor polarization with positive and negative vector polarization, respectively. $\sigma(P,0)$ and $\sigma(-P,0)$ require positive and negative vector polarization while suppressing tensor polarization. Therefore the numerator $(\sigma(P,Q)+\sigma(-P,Q))$ will cancel the vector contribution, leaving only the unpolarized and tensor contributions; and the denominator $(\sigma(P,0)+\sigma(-P,0))$ is equivalent to the unpolarized cross contribution.

A similar approach was implemented in the inclusive experiment aimed at measuring the tensor asymmetry in the Quasi-Elastic region (reference [54]). As discussed in Section 2.2, these spin transitions can be accomplished quickly, reducing the impact of long-term detector or beam current fluctuations on extracting A_{zz}. Furthermore, the uniform magnetic field needed for all states will ensure similar acceptance corrections and cancel out in the ratio.

The kinematics access $Q^2 > 1.5$ GeV^2 with minimal FSI contributions. However, the aperture of the target magnet is $\pm 35°$, and this constrains the kinematic region we can access. In the optimization of kinematics for the desired region, we chose $\theta_e = 7.6°$ and $\theta_p = 52.34°$, as explained in Section 3.3. Under these requirements the magnetic field will be rotated to a $\theta_{\vec{B}} = 20°$towards the HMS, as shown in Fig. 8. Theoretical predictions have been adjusted accordingly to align with the direction of polarization [39].

Since many factors will cancel in the polarized and unpolarized cross-section ratios, the asymmetry will be described by,

$$A_{zz} = \frac{2}{fP_{zz}}\frac{N_p - N_u}{N_u} \tag{11}$$

where f is the dilution factor, $N_p \sim N(P,Q) + N(-P,Q)$ and $N_u \sim N(P,Q) + N(-P,Q)$ are the polarized and unpolarized number of events.

We will also observe scattering events from Deuterium (D), Nitrogen (N), and helium-4 (^4H_e). This is because our target, ammonia (ND_3), is immersed in a helium-4 bath, along with other nuclei present in the setup (such as the scattering chamber, target cup, NMR coils, etc). Consequently, the dilution factor that adjusts for the presence of these nuclei is

$$f = \frac{N_D \sigma_D}{N_D \sigma_D + N_N \sigma_N + \sum_A N_A \sigma_A} \tag{12}$$

where N_D, N_N and N_A are the number of nuclei present in the target ,and σ_D, σ_N and σ_A the cross section for D, N and the other nuclei respectively.

We have studied in the proposed kinematics the dilution factor by accounting for the ^{14}N and ^{4}He contributions. Fig. 12 shows the projected dilution factor as a function of the missing momentum for different θ_{nq} bins, assuming 85 nA and 8 weeks of running. A minimum is observed around 0.21 GeV, after which it begins to rise with the missing momentum to $\sim$0.3 and continues to rise more gradually for recoil angles $\theta_{nq} > 50$.

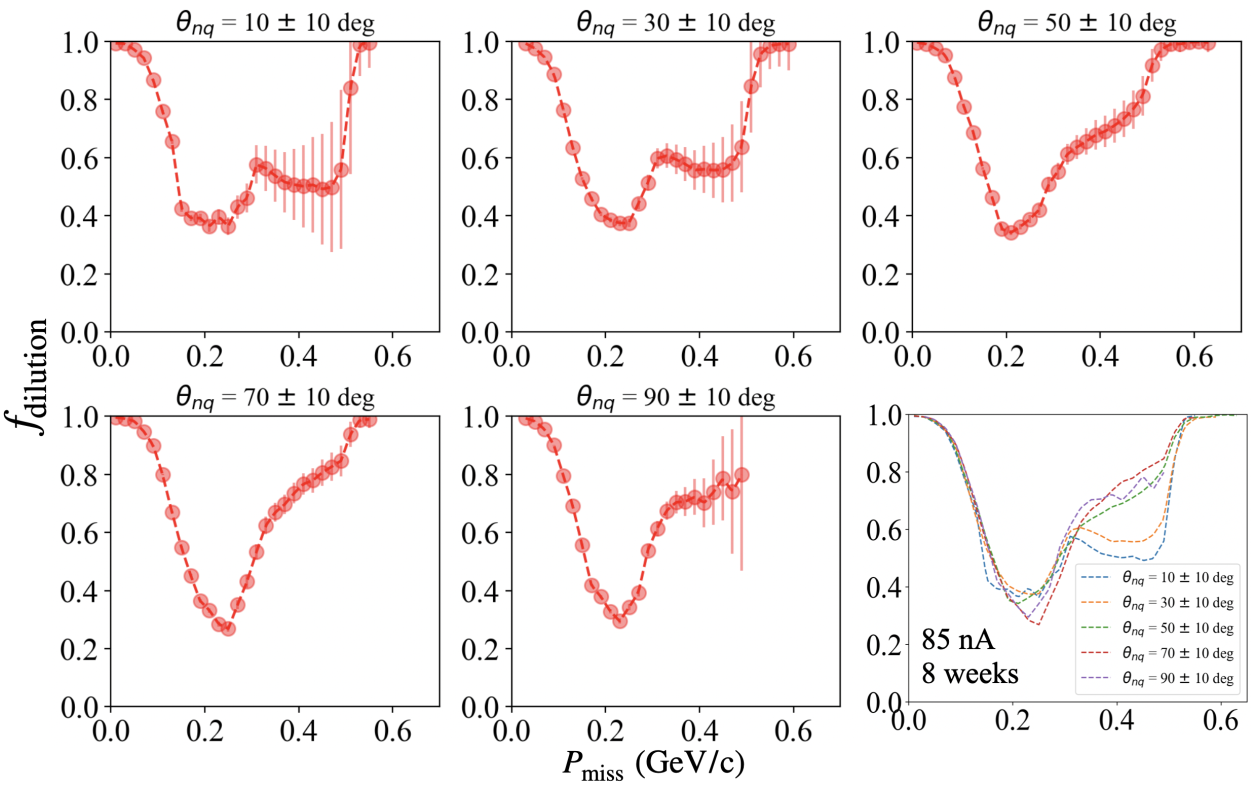

Figure 12: dilution factor vs. missing momentum binned in separate θ_{nq} bins and overlay of interpolated dilution factors (last panel).

3.2 Nodes asymmetry

The uniqueness of the tensor target lets us access ρ_{nodes}, as shown in Eq. 4. In terms of our measured asymmetry A_{zz}, described in Eq. 5, we can rewrite it as the asymmetry,

$$A_{node} = \left(1 - \frac{4}{(3\cos^2\theta_N - 1)Q}\right) + \frac{4}{(3\cos^2\theta_N - 1)Q}\left(\frac{\sigma(P,Q) + \sigma(-P,Q)}{\sigma(P,0) + \sigma(-P,0)}\right) \tag{13}$$

We chose to use cross-section ratios because we will take the advantage of canceling systematic effects. We can also write R_{nodes} in terms of the tensor asymmetry,

$$A_{node} = 1 + \frac{2}{(3\cos^2\theta_N - 1)}A_{zz} \tag{14}$$

Measure the nodes location which is very interesting by itself, we will use the second node to distinguish NN potentials, since they disagree most at larger momentum (see Section 3.4).

3.3 Simulations

The standard Hall C $A(e,e'p)$ coincidence simulation package (SIMC) was used to estimate the count rates for electron-scattering off a 3-cm long ammonia (ND_3) target immersed in a helium-4 bath. Since electrons could scatter off deuterium (^{2}H), nitrogen (^{14}N) or helium (^{4}He), the simulation was done independently for $d(e,e'p)$, ^{4}He$(e,e'p)$ and ^{12}C$(e,e'p)$ reactions, respectively. The carbon was scaled to nitrogen. The deuteron reaction used the J.M. Laget FSI model (using the Paris NN potential) [55], whereas the helium and carbon reactions used the O. Benhar spectral functions (SF). See Table 2 for summary of the target parameters used.

target	$\rho_{t,\text{eff}}$ (g/cm^3)	N_{amu} (g/mol)	$\sigma_{t,\text{eff}}$ (mg/cm^2)	abundancy (packing fraction)	T_N (transparency)
^{2}H	0.303	2.0141	910.5	0.65	1
^{4}He	0.141	4.0026	423.6	0.35	0.72
^{14}N	0.704	14.0067	2110.5	0.65	0.53
^{12}C	1.8	12.0107	573.8	–	0.55

Table 2: SIMC target parameters

Effective target areal thickness:

To account for electrons scattering off individual nitrogen and deuteron nuclei in ND_3, an effective target density was determined for each target as follows:

$$\rho^{d}_{t,\text{eff}} = \rho_{\text{ND}_3} \cdot (3\text{N}_{\text{d,amu}})/\text{N}_{\text{ND}_3\text{,amu}} \text{ (deuteron)}$$
$$\rho^{n}_{t,\text{eff}} = \rho_{\text{ND}_3} \cdot (\text{N}_{^{14}\text{N,amu}})/\text{N}_{\text{ND}_3\text{,amu}} \text{ (nitrogen)}$$

where $\rho_{t,\text{eff}}$ are the effective target densities and N_{amu} are the targets molar masses. For ND_3, these values are (1.007 g/cm^3, 20.049 g/mol). For helium, since it is not part of the solid target, the standard ^{4}He density was used. The effective target thickness ($\sigma_{t,\text{eff}}$) was then determined by multiplying the densities by the 3-cm target length.

Scaling c12 to n14:

Since there is no ^{14}N model in SIMC, the Benhar SF for ^{12}C was used instead. The Hall C carbon foil target thickness used in the CaFe experiment was used as input in the initial simulation, and the yield was then scaled to nitrogen by the target thickness and nuclear transparency [56] as follows:

$$Y_{\text{n14}} = Y_{\text{c12}} \times \frac{\sigma^{(\text{n14})}_{t,\text{eff}}}{\sigma^{(\text{c12})}_{t,\text{eff}}} \times \frac{T^{(\text{n14})}_{N}}{T^{(\text{c12})}_{N}}$$

Other simulation effects:

To have a more realistic estimate of the count rates, (i) *radiative*, (ii) *energy loss*, and a (iii) *target magnetic field* effects were also included in the simulation. Radiative effects can significantly change the electron kinematics and therefore the measured yields, due to the emission of *bremsstrahlung* photons near the target field. Energy loss effects account for the particles passage through the detector/spectrometer entrance and exit windows which also leads to a measurable effect in the yields. Finally, a target magnetic field map was calculated by J. Benesch [46] and implemented in the simulation to study the effects on the particle trajectories due to the 5T solenoid polarization magnet.

Event-selection cuts:

To select $d(e, e'p)$ coincidence events, we used the standard definition of missing energy in: $E_{\text{miss}} = \nu - T_p - T_{\text{rec}}$, where ν is the energy transferred to the nucleus, and (T_p, T_{rec}) are the proton and recoil kinetic energies, respectively. For the special case of a deuteron break-up reaction, the recoil kinetic energy refers to that of the neutron. Since the deuteron has no excited states, the kinetic energies of the proton and neutron are well-defined and the missing energy becomes the binding energy of the deuteron, ~ 2.2 MeV. Due to the finite energy resolution of the spectrometers, however, the binding energy of the deuteron is spread about its central value. In addition, spectrometer momentum ($\Delta P/P_0$) and angular acceptance cuts were also applied. The momentum acceptance refers to a relative variation of the detected particle momentum, ΔP with respect to the spectrometer central momentum, P_0, and the angular acceptance refers to a relative variation in the scattered particles in-plane and out-of-plane angles with respect to the central spectrometer angle. The events are reconstructed and projected back to a collimator where the angular acceptance cut is applied. A summary of the cuts applied is presented in Table 3. The kinematics distributions are shown in 3.3.1.

E_{miss}	-10 to 40 MeV
HMS $\Delta P/P_0$	-10 to 10 %
SHMS $\Delta P/P_0$	-10 to 22 %
HMS collimator	octagonal

Table 3: SIMC event-selection cuts

Background contributions:

To estimate the experimental background contributions from electrons scattering off ^{14}N in ND_3 or ^{4}He from the target helium bath, the exact same analysis cuts were applied to these target nuclei as well. The calculations of the kinematic variables for the background assumed the deuteron target mass, similar to what is done as a standard procedure for the subtraction of Aluminum endcaps in cryotargets, where the mass of the target is assumed.

Yield + background rate estimates:

The simulation assumed an 11-GeV, 85-nA incident electron beam on each of the targets (^{2}H, ^{4}He, ^{14}N) for a beam-on-target period of 2 weeks each (336 hrs). This specific time was chosen (see Section5), as the experiment will be divided into four different 2-week-long target polarization configurations, for a total of 8-weeks beam-on-target for the bulk of the experiment (excluding overhead time), as required by the A_{zz} measurement described in Section3.1. The 2-week statistical projections are used in the determination of the uncertainties in each of the four polarization states and subsequently in the A_{zz} uncertainty projections described in Section 3.4

target	$(e,e'p)$ counts	$(e,e'p)$ rates (counts/hr)	DAQ rates (Hz)	relative $(e,e'p)$ counts (%)
^{2}H	745,564	2,219	1.02	–
^{4}He	2,284	7	0.006	0.31
^{14}N	70,556	210	0.123	9.4

Table 4: SIMC yield (^{2}H) and background (^{4}He, ^{14}N) rate estimates for a 2-week (336 hrs) beam-on-target period at 85 nA. Data-Acquisition (DAQ) rates exclude analysis cuts. The last column are the relative (to deuterium) background contribution in percent

The following subsections show the relevant kinematic and acceptance variables for ^{2}H$(e,e'p)$, ^{4}He$(e,e'p)$ and ^{14}N$(e,e'p)$ reactions with all event-selection cuts (Table3) applied for 336 hrs beam-on-target at 85 nA. Note in some of the histograms, the strips of color blue are a result of Nitrogen(N14, blue) not being directly overlaid with deuterium (D2, yellow). The green strips are when both are directly overlaid, hence blue+yellow forms green. The presence of Helium (magenta) is almost non-existent, as indicated by the arrows pointing to it.

3.3.1 Kinematics

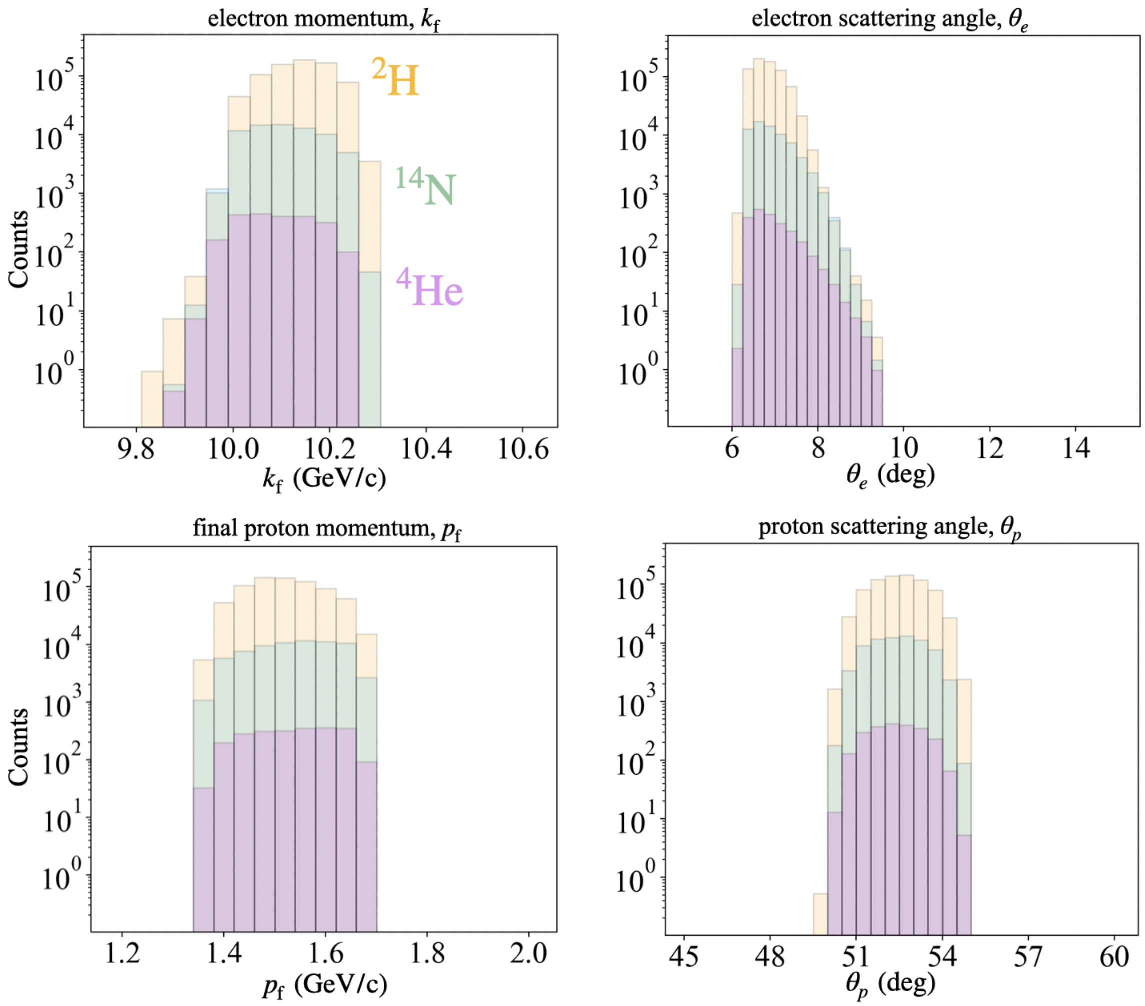

Figure 13: Simulated spectrometer kinematic distributions for SHMS (electrons) and HMS (protons) for 336 hrs at 85 nA.

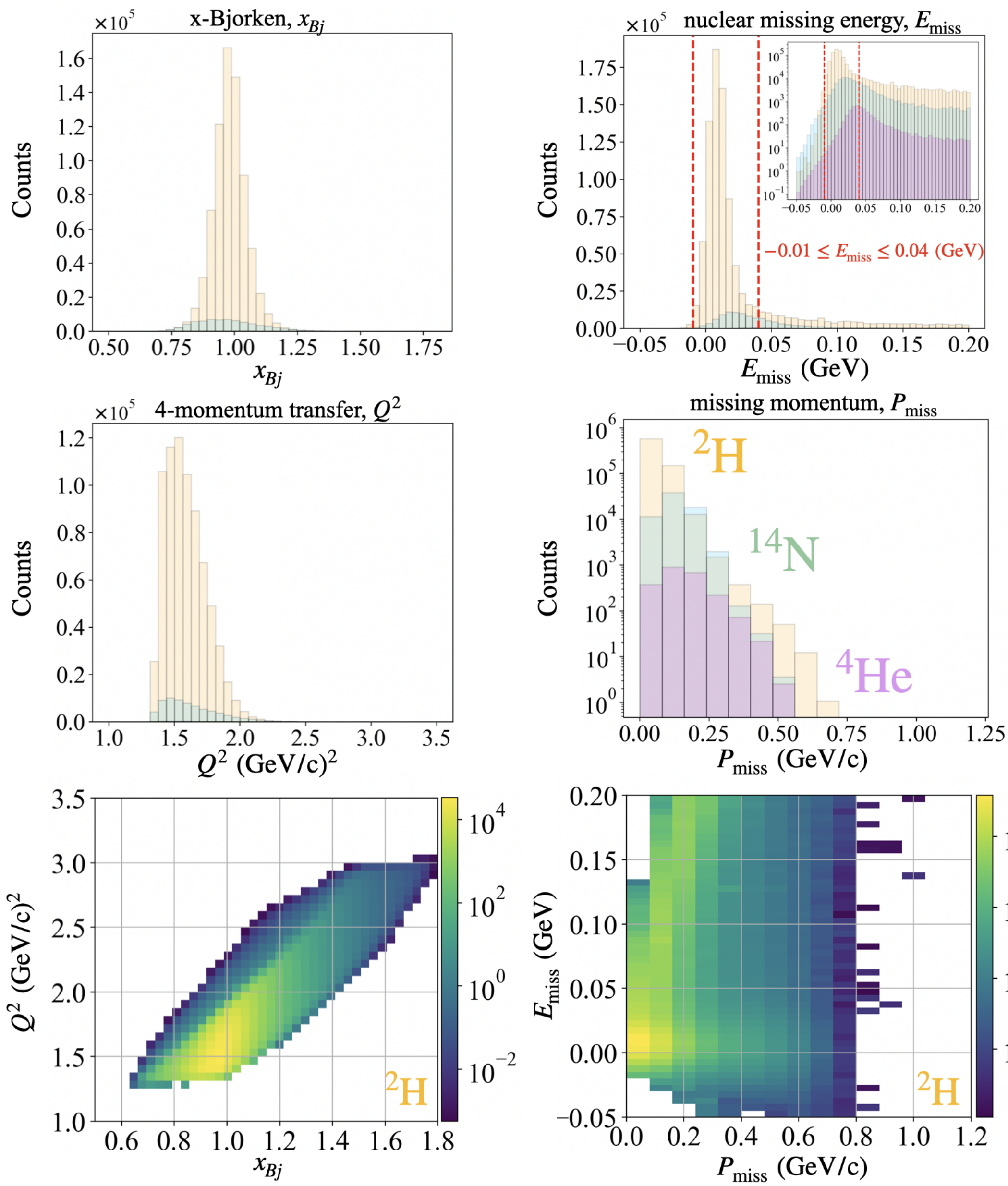

Figure 14: Additional kinematic distributions for 336 hrs at 85 nA. (bottom 2 panels) 2D correlations of Q^2 vs. x_{Bj} (left) and E_{miss} vs. P_{miss} only for ^{2}H. The color bar indicates the counts.

3.3.2 Acceptance

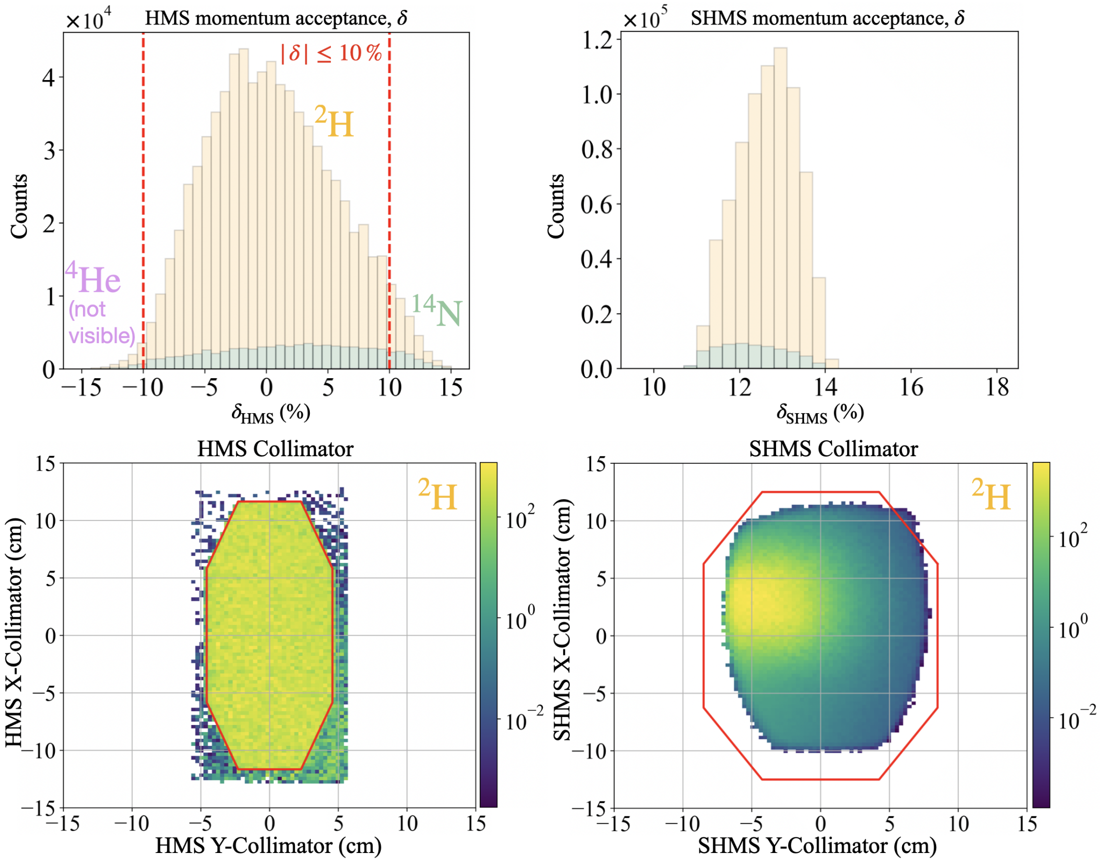

Figure 15: Momentum (top) and angular (bottom) acceptance for 336 hrs at 85 nA. The bottom panels show a contour line indicating the collimator geometry boundary; the HMS collimator determine the acceptance of the SHMS, as evidenced by most events in SHMS acceptance falling within the collimator geometry.

3.3.3 Yields

The simulation yield (and relevant observables presented in Section 3.4) are binned in terms of (P_{miss}, θ_{nq}). We have opted for this approach because there's a notable angular dependency observed in final-state interactions with the neutron recoil angle, as shown by Ref. [23], where FSIs are strongest at θ_{nq} ~70° whereas they are significantly reduced at more forward angles, θ_{nq} ~30–40°. Therefore, one is able to study how FSIs affect our observables, by isolating its effects for different recoil angles. Furthermore, for forward recoil angles (small FSI), and at larger Q^2 (>1 (GeV/c)^2), the only dominant contribution to the cross section becomes the plane-wave impulse approximation (PWIA) where the proton is knocked-out without further re-interactions between it and the residual system (neutron). In this scenario, the recoil neutron ("missing") momentum P_{miss} is minimally distorted by FSI and therefore, it can be approximated to be the internal momentum of the bound proton, thereby allowing a direct access to the internal nucleon momenta.

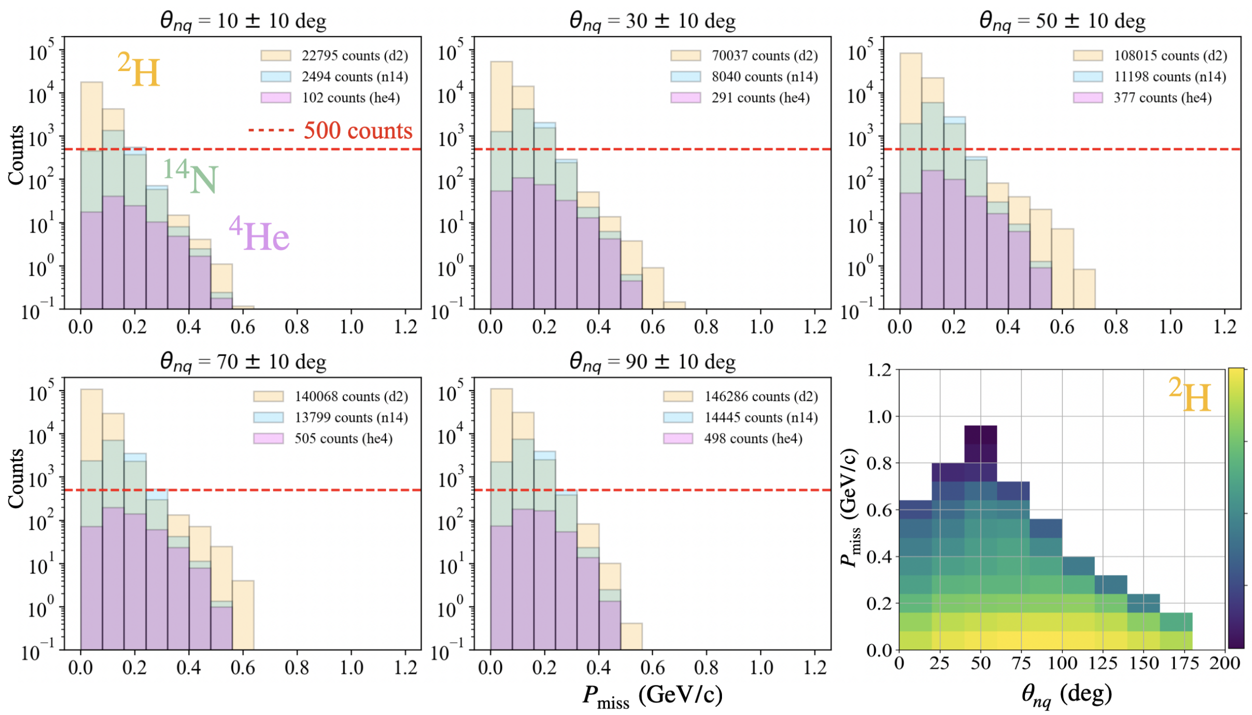

Figure 16: The first 5 panels show the yield binned in missing momentum (P_{miss}) for different neutron recoil angles (θ_{nq}). The last panel shows a 2D correlation of P_{miss} vs. θ_{nq} for deuterium. The dashed red line is a reference indicating the counts required for producing a reasonable uncertainty in the A_{zz} asymmetry.

3.4 Projected results

The proposed experiment accesses the region of $0.1 < P_m < 0.5$ GeV/c with angles $\theta_{nq} < 90°$. The beauty of this experiment relies on large asymmetries with regions of large difference between the NN potentials. In the following projections 1718, the dashed lines are PWIA and the solid full calculations with FSI [39]. The dark orange are calculations using CD-Bonn and the green use AV18.

The nodes asymmetry is organized into bins for P_m for a θ_{nq} bin, as shown in Fig. 18. It's crucial to highlight that our experiment will mark the first attempt at probing the u-wave of the deuteron at Jefferson Lab using this method; previous measurements did not reach such high momentum transfers (refer to Section 1.2.3). This analysis will allow us to investigate the nodes, with the first node exhibiting consistency across the two considered NN potentials, while the second node can vary significantly depending on the chosen potential. Thus, our measurements at $0 < \theta_{nq} < 40°$ will precisely examine the discrepancy between these two NN potentials.

In addition, the other data points will test FSI, since the theory calculations seem to agree for both NN potentials (See Fig. 17a, particularly the points at lower $40 < \theta_{nq} < 75°$).

The lowest momentum data points ($0.1 < P_m < 0.26$ GeV/c) in A_{node} are regions where at low $\theta_{nq} < 40°$ the FSI are minimal and the NN potentials agree. Those regions will help us to test the consistency of our measurement compared with the theory predictions.

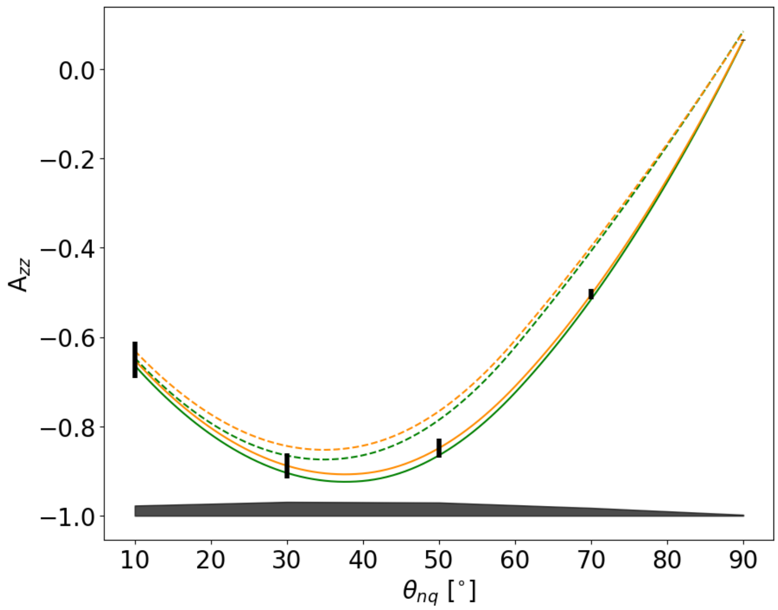

(a)

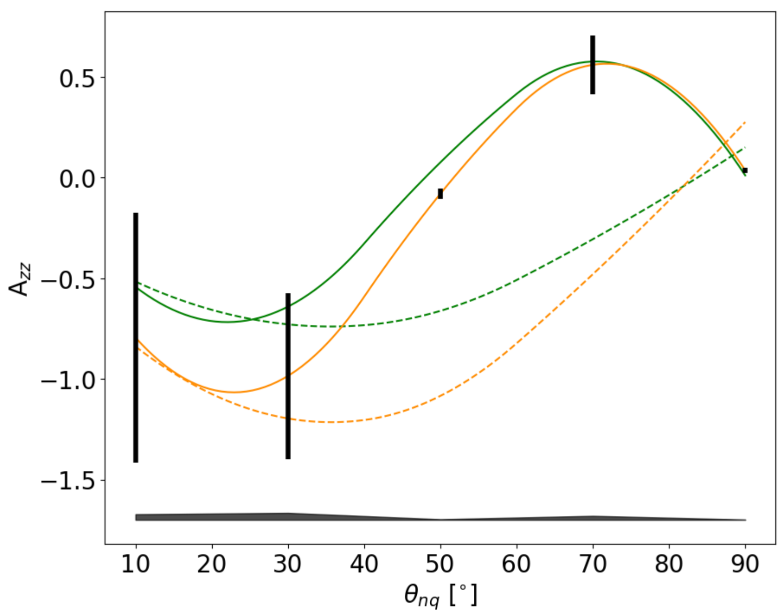

(b)

Figure 17: Expected results of the tensor asymmetry A$_{zz}$ with respect to the θ_{nq}. The calculations used the AV18 and CD-Bonn NN potentials, represented by green and orange lines, respectively. Dashed lines denote PWIA calculations, while solid lines indicate full calculations with FSI. The energies for the panels are as follows: (a) $0.08 < P_m < 0.24$ GeV, (b) $0.32 < P_m < 0.48$ GeV.

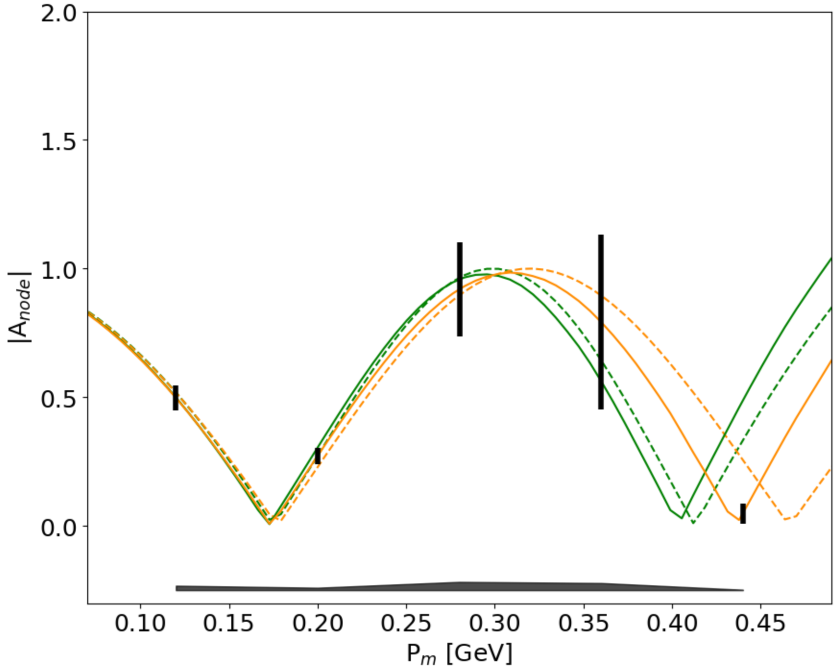

(a)

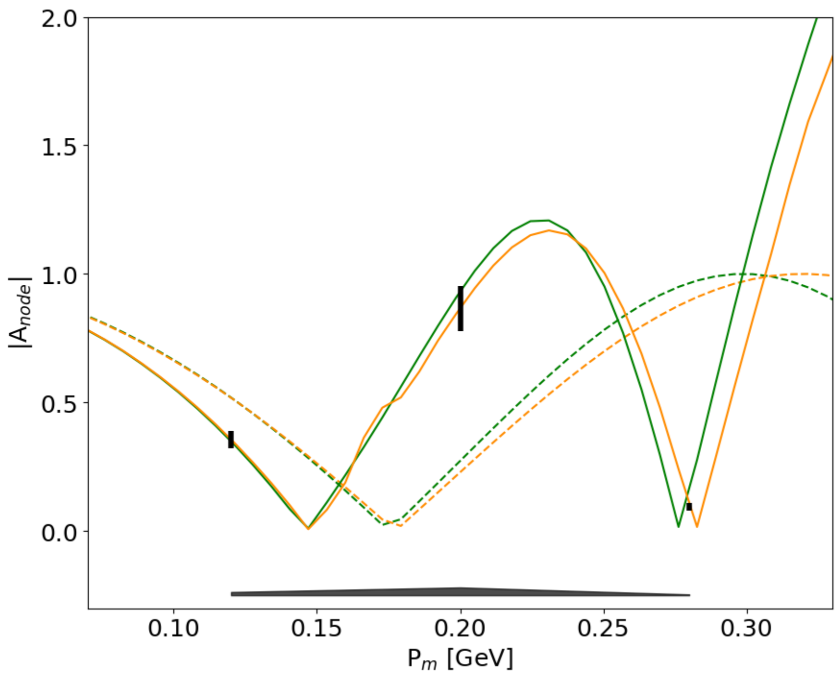

(b)

Figure 18: Expected results for R_{nodes} with respect to the P_m. AV18 and CD-Bonn were used as nn potentials, represented by gray and black lines, respectively. Dashed lines denote PWIA calculations, while solid lines indicate full calculations with FSI. The energies for the panels are as follows: (a) $0 < \theta_{nq} < 40°$, (b) $60 < \theta_{nq} < 100°$.

4 Measurement Uncertainties

Our spin-1 observables rely on measuring data for four distinct target helicity states using identical experimental setups. Some of the systematic effects will be canceled by taking the ratio of measurements (see equation 10), and it won't affect the absolute normalization. However, while taking the data in the different states, detector drifts, detector changes, or any possible fluctuation may imply effects that do not cancel out in the ratio.

Our proposed experimental configuration adopts a methodology akin to that of the E12-15-005 [49] and E12-13-011 [48] experiments. Notable modifications include a 20°rotation of the magnetic field and the utilization of the HMS for proton detection.

Based on the studies done by those collaborations and the results of previous experiments that used the same polarized target [57–60]. We anticipate that the primary systematic uncertainties will arise from polarization measurements as well as dilution and packing fraction considerations, as summarized in table 5. The uncertainties related to polarization, dilution, and packing fraction are added to the point-to-point uncertainties in the projected results 3.4, while other uncertainties are included in the error band of the Fig. 17 and 18.

Source	(%)
Polarization	7
Dilution and Packing fraction	6
Radiative corrections	3
Charge determination	1
Trigger/tracking Efficiency	1
Acceptance	0.5

Table 5: Major sources of systematic uncertainties

4.1 Point-to-point uncertainties

The point-to-point uncertainties accounted in the plots include statistical, polarization and dilution effects. It is defined as,

$$\delta A_{zz} = \sqrt{\delta A_{zz}^{stat} + \delta A_{zz}^{P_{zz}} + \delta A_{zz}^{f}}, \tag{15}$$

where δA_{zz}^{stat} is due to the statistic effects, $\delta A_{zz}^{P_{zz}}$ is due to the polarization and δA_{zz}^{f} to the dilution factor.

The systematic contribution was defined as,

$$\delta A_{zz}^{stat} = \frac{2}{P_{zz}} \sqrt{\left(\frac{\sqrt{N_p}}{N_u}\right)^2 + \left(\frac{N_p \sqrt{N_u}}{N_u^2}\right)^2} \tag{16}$$

since our measurement asymmetry goes as Eq. eq:Azz.

The polarization techniques used to enhance the tensor polarization are expected to have a maximum relative 7% uncertainty. We will measure the polarization using the lineshape techniques developed by the University of Virginia. The work in [50] summarizes the techniques used in the lineshape analysis. The polarized target groups of the University of Virginia and the University of New Hampshire are part of our collaboration and will support the target developments for this experiment.

In addition, the dilution factor varies with missing momentum in our experiment, and our simulations indicate that it reaches a minimum value around $P_{\text{miss}} \sim 2.5$ GeV/c, while remaining above 0.5 for $P_{\text{miss}} \gtrsim 0.3$ GeV/c . It's crucial to have precise knowledge of the dilution factor at every kinematic point, and this information should be derived from empirical data with quantifiable error. Hence, in the run plan, we anticipate conducting measurements with both C and empty cell runs, aiming to attain a level of precision comparable to that of previous experiments such as [57] in Hall A.

4.2 Normalization uncertainties

The next major effect we expect to encounter is related to radiative effects, which necessitate investigations into both polarized and unpolarized corrections for the proposed kinematic region. We anticipate that these effects will remain within the bounds reported in previous experiments, such as [57], which noted a 3% effect.

In addition, we will use the same beam current monitors (BCMs) as the approved E12-15-005 [49] and E12-13-011 [48] experiments for charge measurements. Despite frequent calibrations, a slight variation in the BCM response during a single helicity flip iteration can lead to a drift of approximately 1×10^{-4}. Accurate temperature monitoring of the BCM's stainless steel pillbox resonant cavity during operation is necessary. Regular calibrations of the BCM and continuous monitoring of detector signals and normalized yield will aid in identifying any potential drift in the devices.

Effects from the detectors, triggers, cuts, and tracking efficiency can introduce errors in normalization; all polarization states experience similar stochastic fluctuations throughout a cycle, resulting in only a minor relative uncertainty in the observable. To mitigate drifts, the polarization states will be switched every 30 minutes. An additional assessment was derived from the stability of the HRS detector, utilizing Hall A transversity data for detected pions, which revealed a drift of 2.2×10^{-4}. To address this, detector thresholds will be cautiously set, and meticulous online monitoring and checks will be employed to track relative changes in tracking efficiency between slugs. Considering trigger, tracking, cuts, and detector errors that directly impact contributions to the uncertainty, we expect the impact will not be larger than 2.2×10^{-4}.

5 Run Plan

We are requesting a total of 56 PAC days with an 11 GeV beam energy and no changes to the spectrometers. Additionally, we are requesting 26 days of overhead, primarily allocated for target spin manipulation purposes. The SHMS will detect the electrons, and it will be centered at $\theta_e = 7.61°$ and $k_f = 9.0$ GeV; the HMS will measure the protons, and it will be centered at $\theta_p = 52.34°$ and $p_f = 1.520$ GeV, as summarized in Table 1.

We estimate the count rate of the experiment by accounting the deuteron, ^4He and N, as described in Section 3.3.Approximately 85% of the total events originate from deuteron. The anticipated total rate is 1 Hz.

5.1 Overhead

Figure 19 shows the gantt chart for the run plan of the proposed experiment. It was generated assuming 85 nA beam current, and assuming the target ladder will have two target cups. Each target cup has a radius of 1.5 cm and length of 3 cm. The dose between anneals is 5.25×10^{15} e/cm^2 and the time required for annealing is an hour. The cups will be replaced once the accumulated dose in the material reaches 4×10^{16} e/cm^2.

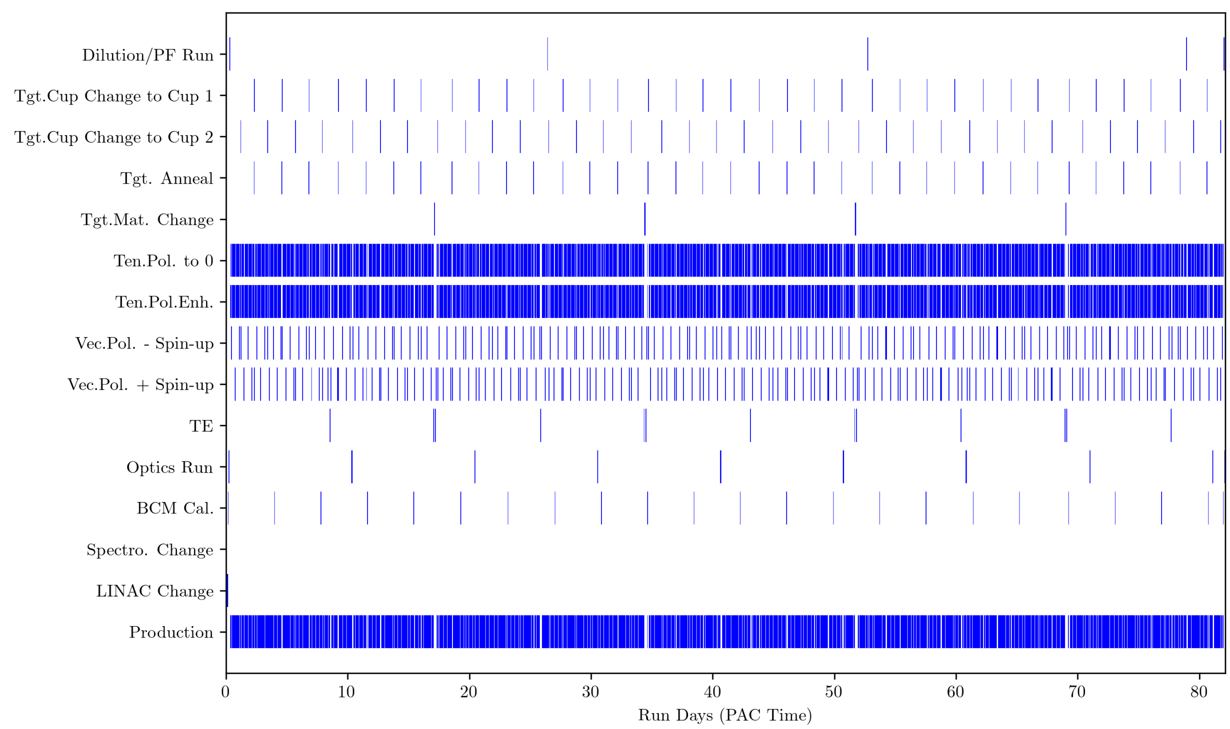

Figure 19: Gannt chart of the run plan for the proposed experiment.

The duration for tensor enhancement and tensor unpolarized states is expected to be a few seconds, with cycles of tensor enhancement and unpolarized states lasting for 1 hour Additionally, TE measurements are scheduled every 12 days, along with runs for packing fraction and dilution, which are empty cell and carbon target runs. The majority of time is allocated to spinning up the target during target changes, estimated to take a total of 21 days. The vector polarization has a time constant of 50 minutes, requiring about 4 time constants for full polarization.

Overhead activities include BCM calibrations every seven days, optics runs spaced every 20 days, and tasks such as target material swaps and target cup changes.

6 Summary

This proposal aims to measure for first time in Jefferson Lab the exclusive electrodisintegration of the deuteron using a polarized target, $D(e,e'p)n$ in Hall C. The kinematic region will focus in $1.5 < Q^2 = 2.5$ GeV^2, wich will cover a region of $0.1 < P_m < 0.5$ GeV and $0 < \theta_{nq} < 90°$. We will learn about the NN potential in the transition to even smaller inter-nucleon distances, and we will be able to place tight constraints on the models and descriptions using the novel measurement technique.

The distinction between the various NN potential descriptions is distinct at high missing momenta (exceeding 0.4 GeV) due to a poor descriptions of the D-wave component. The prevalence of the tensor interaction in the high-momentum segment of the nuclear wave function may exert a significant influence on the dynamics of asymmetric nuclei, leading to nontrivial implications for superdense nuclear matter and neutron stars.

Furthermore, we will have the opportunity to examine final-state interactions (FSI) at various θ_{nq} within the $0 < P_m < 0.5$ GeV range. These investigations are crucial for gaining a thorough understanding of FSI in other types of reactions.

Achieving the physics goals will require a total of 56 PAC days with an 11 GeV beam energy and 26 days of overhead. The 56 PAC days will be divided evenly in the four polarization states we required $(R(P,Q), R(-P,Q), R(P,0), R(-P,0))$ and the polarization states will be changed regularly to mitigate the drift uncertainties that may happen during the experiment. We foresee the major contributions of uncertainty to our measurement beyond the statistics in some of our kinematics points will be attributed to our knowledge of the polarization and the dilution factor.

References

[1] E. Piasetzky, M. Sargsian, L. Frankfurt, M. Strikman and J. W. Watson, *Evidence for the strong dominance of proton-neutron correlations in nuclei*, *Phys. Rev. Lett.* **97** (2006) 162504, [nucl-th/0604012].

[2] R. Subedi et al., *Probing Cold Dense Nuclear Matter*, *Science* **320** (2008) 1476–1478, [0908.1514].

[3] M. M. Sargsian, *New properties of the high-momentum distribution of nucleons in asymmetric nuclei*, *Phys. Rev. C* **89** (2014) 034305, [1210.3280].

[4] O. Hen et al., *Momentum sharing in imbalanced Fermi systems*, *Science* **346** (2014) 614–617, [1412.0138].

[5] CLAS collaboration, M. Duer et al., *Probing high-momentum protons and neutrons in neutron-rich nuclei*, *Nature* **560** (2018) 617–621.

[6] J. L. Friar, *Measurability of the deuteron D state probability*, *Phys. Rev. C* **20** (1979) 325–330.

[7] R. D. Amado, M. P. Locher and M. Simonius, *Asymptotic normalization of the deuteron D state*, *Phys. Rev. C* **17** (1978) 403–405.

[8] V. G. J. Stoks, R. A. M. Klomp, C. P. F. Terheggen and J. J. de Swart, *Construction of high quality N N potential models*, *Phys. Rev. C* **49** (1994) 2950–2962, [nucl-th/9406039].

[9] M. Lacombe, B. Loiseau, R. Vinh Mau, J. Cote, P. Pires and R. de Tourreil, *Parametrization of the deuteron wave function of the Paris n-n potential*, *Phys. Lett. B* **101** (1981) 139–140.

[10] R. Machleidt, *The High precision, charge dependent Bonn nucleon-nucleon potential (CD-Bonn)*, *Phys. Rev. C* **63** (2001) 024001, [nucl-th/0006014].

[11] R. B. Wiringa, V. G. J. Stoks and R. Schiavilla, *An Accurate nucleon-nucleon potential with charge independence breaking*, *Phys. Rev. C* **51** (1995) 38–51, [nucl-th/9408016].

[12] L. L. Frankfurt and M. I. Strikman, *Relativistic Description of the Deuteron: Elastic and Inelastic Form-Factors in the Region Kinematically Forbidden for Scattering on a Free Nucleon*, *Nucl. Phys. B* **148** (1979) 107–140.

[13] W. W. Buck and F. Gross, *A Family of Relativistic Deuteron Wave Functions*, *Phys. Rev. D* **20** (1979) 2361.

[14] J. Carbonell, B. Desplanques, V. A. Karmanov and J. F. Mathiot, *Explicitly covariant light front dynamics and relativistic few body systems*, *Phys. Rept.* **300** (1998) 215–347, [nucl-th/9804029].

[15] G. A. Miller, *Light front quantization: A Technique for relativistic and realistic nuclear physics*, *Prog. Part. Nucl. Phys.* **45** (2000) 83–155, [nucl-th/0002059].

[16] M. Harvey, *Effective nuclear forces in the quark model with Delta and hidden color channel coupling*, *Nucl. Phys. A* **352** (1981) 326–342.

[17] C.-R. Ji and S. J. Brodsky, *Quantum Chromodynamic Evolution of Six Quark States*, *Phys. Rev. D* **34** (1986) 1460.

[18] V. G. Neudachin, Y. F. Smirnov and R. Tamagaki, *An Explanation of n n Repulsive Core in Terms of Forbidden States Based on the Quark Model*, *Prog. Theor. Phys.* **58** (1977) 1072.

[19] A. Faessler, F. Fernandez, G. Lubeck and K. Shimizu, *The Quark Model and the Nature of the Repulsive Core of the Nucleon Nucleon Interaction*, *Phys. Lett. B* **112** (1982) 201–205.

[20] R. A. Gilman and F. Gross, *Electromagnetic structure of the deuteron*, *J. Phys. G* **28** (2002) R37–R116, [nucl-th/0111015].

[21] J. Arrington, D. W. Higinbotham, G. Rosner and M. Sargsian, *Hard probes of short-range nucleon-nucleon correlations*, *Prog. Part. Nucl. Phys.* **67** (2012) 898–938, [1104.1196].

[22] CLAS collaboration, K. S. Egiyan et al., *Experimental study of exclusive H-2(e,e-prime p)n reaction mechanisms at high Q**2*, *Phys. Rev. Lett.* **98** (2007) 262502, [nucl-ex/0701013].

[23] Hall A collaboration, W. U. Boeglin et al., *Probing the high momentum component of the deuteron at high Q^2*, *Phys. Rev. Lett.* **107** (2011) 262501, [1106.0275].

[24] W. Boeglin and M. Sargsian, *Modern Studies of the Deuteron: from the Lab Frame to the Light Front*, *Int. J. Mod. Phys. E* **24** (2015) 1530003, [1501.05377].

[25] L. L. Frankfurt, W. R. Greenberg, G. A. Miller, M. M. Sargsian and M. I. Strikman, *Color transparency effects in electron deuteron interactions at intermediate Q**2*, *Z. Phys. A* **352** (1995) 97–113, [nucl-th/9501009].

[26] L. L. Frankfurt, M. M. Sargsian and M. I. Strikman, *Feynman graphs and Gribov-Glauber approach to high-energy knockout processes*, *Phys. Rev. C* **56** (1997) 1124–1137, [nucl-th/9603018].

[27] M. M. Sargsian, *Selected topics in high energy semiexclusive electronuclear reactions*, *Int. J. Mod. Phys. E* **10** (2001) 405–458, [nucl-th/0110053].

[28] C. Ciofi degli Atti and L. P. Kaptari, *Calculations of the exclusive processes H-2(e, e-prime p)n, He-3(e, e-prime p)H-2 and He-3(e, e-prime p)(pn) within a generalized Glauber approach*, *Phys. Rev. C* **71** (2005) 024005, [nucl-th/0407024].

[29] J. M. Laget, *The Electro-disintegration of few body systems revisited*, *Phys. Lett. B* **609** (2005) 49–56, [nucl-th/0407072].

[30] S. Jeschonnek and J. W. Van Orden, *A New calculation for D(e, e-prime p)n at GeV energies*, *Phys. Rev. C* **78** (2008) 014007, [0805.3115].

[31] M. M. Sargsian, *Large Q**2 Electrodisintegration of the Deuteron in Virtual Nucleon Approximation*, *Phys. Rev. C* **82** (2010) 014612, [0910.2016].

[32] W. P. Ford, S. Jeschonnek and J. W. Van Orden, $^2H(e, e'p)$ *observables using a Regge model parameterization of final state interactions*, *Phys. Rev. C* **87** (2013) 054006, [1304.0647].

[33] Hall C collaboration, C. Yero et al., *Probing the Deuteron at Very Large Internal Momenta*, *Phys. Rev. Lett.* **125** (2020) 262501, [2008.08058].

[34] M. M. Sargsian and F. Vera, *New Structure in the Deuteron*, *Phys. Rev. Lett.* **130** (2023) 112502, [2208.00501].

[35] CLAS collaboration, M. Duer et al., *Direct Observation of Proton-Neutron Short-Range Correlation Dominance in Heavy Nuclei*, *Phys. Rev. Lett.* **122** (2019) 172502, [1810.05343].

[36] CLAS collaboration, A. Schmidt et al., *Probing the core of the strong nuclear interaction*, *Nature* **578** (2020) 540–544, [2004.11221].

[37] R. Cruz-Torres, D. Lonardoni, R. Weiss, N. Barnea, D. W. Higinbotham, E. Piasetzky et al., *Many-body factorization and position–momentum equivalence of nuclear short-range correlations*, *Nature Phys.* **17** (2021) 306–310, [1907.03658].

[38] M. M. Sargsian and M. I. Strikman, *Inclusive and Exclusive Scatterings from Tensor Polarized Deuteron*, *J. Phys. Conf. Ser.* **543** (2014) 012009, [1409.6056].

[39] M. Sargsian, *Tensor polarization structure functions*, *Private communication* (2024) .

[40] M. M. Sargsian, *Non-nucleonic degrees of freedom and the spin structure of the deuteron*, in *25th International Spin Symposium*, 2, 2024. 2402.13458.

[41] Z. L. Zhou et al., *Tensor analyzing powers for quasielastic electron scattering from deuterium*, *Phys. Rev. Lett.* **82** (1999) 687–690, [nucl-ex/9809002].

[42] A. DeGrush et al., *Measurement of the Vector and Tensor Asymmetries at Large Missing Momentum in Quasielastic* $(\vec{e}, e'p)$ *Electron Scattering from Deuterium*, *Phys. Rev. Lett.* **119** (2017) 182501, [1707.03028].

[43] Blast collaboration, R. Milner, *Measurement of the Vector and Tensor Asymmetries at Large Missing Momentum in Quasielastic* $(\vec{e}, e'p)$ *Electron Scattering from Deuterium*, *PoS* **SPIN2018** (2019) 026.

[44] L. L. Frankfurt, M. I. Strikman, D. B. Day and M. Sargsian, *Evidence for short range correlations from high Q**2 (e, e-prime) reactions*, *Phys. Rev. C* **48** (1993) 2451–2461.

[45] N. Fomin et al., *New measurements of high-momentum nucleons and short-range structures in nuclei*, *Phys. Rev. Lett.* **108** (2012) 092502, [1107.3583].

[46] J. Benesch, *Proof of principle design for pre-chicane for use with 5t transverse solenoid for high current in hall c, small shms angles in hall c, or solid, tn-24-007*, tech. rep., 2024.

[47] J. Benesch, *Supplement: Proof of principle design for pre-chicane for use with 5t transverse solenoid for high current in hall c, small shms angles in hall c, or solid, tn-24-007*, tech. rep., 2024.

[48] "K. Slifer, *et al.*, Jefferson Lab PAC40, E12-13-011 (2013).."

[49] "E. Long, *et al.*, Jefferson Lab PAC44, E12-15-005 (2016).."

[50] J. Clement and D. Keller, *Manipulation of spin-1 solid-state targets*, *Nucl. Instrum. Meth. A* **1050** (2023) 168177.

[51] D. Keller, D. Crabb and D. Day, *Enhanced Tensor Polarization in Solid-State Targets*, *Nucl. Instrum. Meth. A* **981** (2020) 164504, [2008.09515].

[52] D. Keller, *Modeling alignment enhancement for solid polarized targets*, *Eur. Phys. J. A* **53** (2017) 155, [1707.07065].

[53] H. Arenhövel, W. Leidemann and E. L. Tomusiak, *Exclusive deuteron electrodisintegration with polarized electrons and a polarized target*, *Phys. Rev. C* **46** (Aug, 1992) 455–470.

[54] "Addressing the Tensor Spin Experiments Conditional Status.."

[55] J. Laget, *The electro-disintegration of few body systems revisited*, *Physics Letters B* **609** (2005) 49–56.

[56] D. Dutta, K. Hafidi and M. Strikman, *Color transparency: Past, present and future*, *Progress in Particle and Nuclear Physics* **69** (2013) 1–27.

[57] Jefferson Lab Hall A g2p collaboration, D. Ruth et al., *Proton spin structure and generalized polarizabilities in the strong quantum chromodynamics regime*, *Nature Phys.* **18** (2022) 1441–1446, [2204.10224].

[58] RSS collaboration, F. R. Wesselmann et al., *Proton spin structure in the resonance region*, *Phys. Rev. Lett.* **98** (2007) 132003, [nucl-ex/0608003].

[59] Jefferson Lab E94010 collaboration, M. Amarian et al., *Measurement of the generalized forward spin polarizabilities of the neutron*, *Phys. Rev. Lett.* **93** (2004) 152301, [nucl-ex/0406005].

[60] O. A. Rondon Aramayo, *The RSS and SANE experiments at Jefferson Lab*, *AIP Conf. Proc.* **1155** (2009) 82–92.